Behavior of Reinforced Concrete Beams subjected to Impact Loading under Large Displacement incorporated with Strain Rate Effect

By

Muhammad Anas

Fall 2019 MS-Structural Engineering

(Registration. No: 00000320874)

NUST Institute of Civil Engineering (NICE)

School of Civil and Environmental Engineering (SCEE)

National University of Sciences and Technology (NUST)

Islamabad, Pakistan

(2023)

Behavior of Reinforced Concrete Beams subjected to Impact Loading under Large Displacement incorporated with Strain Rate Effect

By

Muhammad Anas

(Registration. No: 00000320874)

A thesis submitted to the National University of Sciences and Technology, Islamabad,
in partial fulfillment of the requirements for the degree of

Master of Science in

Structural Engineering

Thesis Supervisor:
Dr. Azam Khan
(Associate Professor)

NUST Institute of Civil Engineering (NICE)

School of Civil and Environmental Engineering (SCEE)

National University of Sciences and Technology (NUST)
Islamabad, Pakistan

BEHAVIOR OF REINFORCED CONCRETE BEAMS SUBJECTED TO IMPACT LOADING UNDER LARGE DISPLACEMENT INCORPORATED WITH STRAIN RATE EFFECT

By

Muhammad Anas

This is to certify that we have examined the above MS thesis and found that it is complete and satisfactory in all respects.

Dr. Azam Khan (Supervisor)	**Dr. Junaid Ahmad** (GEC Member)	**Dr. Hammad Anis** (GEC Member)

THESIS ACCEPTANCE CERTIFICATE

It is certified that the final copy of MS thesis written by **Mr. Muhammad Anas**, Registration No **00000320874**, of **NUST INSTITUTE OF CIVIL ENGINEERING (NICE)** has been vetted by the undersigned, found complete in all respect as per NUST Statutes/Regulations,is free of plagiarism, errors, and mistakes and is accepted as partial fulfillment for the award of MS degree in Structural Engineering.

Signature (Supervisor), Dr. Azam Khan: Associate Professor NUST Institute of Civil Engineering National University of Sciences & Technology (NUST)

Date: _____

Signature (HOD): HoD Structural Engineering NUST Institute of Civil Engineering School of Civil & Environmental Engineering National University of Sciences and Technology

Date: _____

Signature (Associate Dean): Dr. S. Muhammad Jamil Associate Dean NICE, SCEE, NUST

Date: 23/8/2023

Signature (Dean & Principal): _____

Date: 24 AUG 2023 PROF DR MUHAMMAD IRFAN Principal & Dean SCEE, NUST

AUTHOR'S DECLARATION

I Muhammad Anas hereby state that my MS thesis titled **"Behavior of Reinforced Concrete Beams subjected to Impact loading under Large Displacement incorporated with Strain Rate Effect"** is my own work and has not been submitted previously by me for taking any degree from **National University of Sciences and Technology** or anywhere else in the country/ world.

At any time if my statement is found to be incorrect even after I graduate, the university has the right to withdraw my MS degree.

Student/Author Signature: 

Name: Muhammad Anas

PLAGIARISM UNDERTAKING

I solemnly declare that research work presented in the thesis titled **"Behavior of Reinforced Concrete Beams subjected to Impact loading under Large Displacement incorporated with Strain Rate Effect"** is solely my research work with no significant contribution from any other person. Small contribution/ help wherever taken has been duly acknowledged and that complete thesis has been written by me. I understand the zero-tolerance policy of the HEC and National University of Sciences and Technology (NUST) towards plagiarism. Therefore, I as an author of the above titled thesis declare that no portion of my thesis has been plagiarized and any material used as reference is properly referred/cited. I undertake that if I am found guilty of any formal plagiarism in the above titled thesis even after award of MS degree, the University reserves the rights to withdraw/revoke my MS degree and that HEC and the University has the right to publish my name on the HEC/University website on which names of students are placed who submitted plagiarized thesis.

Student/Author Signature: 

Name: Muhammad Anas

ACKNOWLEDGEMENTS

I am thankful to Allah Almighty, The Most Gracious and The Most Bountiful, who gave me the knowledge, strength and patience to complete this dissertation work. Sincere gratitude for my research supervisor, Dr. Azam Khan.

I am extremely grateful to my all GEC committee members for their availability throughout this research work.

Last but not the least; I would like to thank my immediate family members i.e. my father, my mother, my two sisters and close friends for their continuous support and prayers.

ABSTRACT

To examine the behavior of rigid plastic structure several methods have been employed, one of which is the linear complementarity approach. However, numerical model of linear complementarity problems (LCP) under small displacement subjected to extreme dynamic loading model can further be refined to predict exact response of structures. In the current study, a numerical model has been established by incorporating large displacement along with the strain rate effect by taking into account the nonlinearity of geometry due to axial forces in an RCC beam in order to obtain precise and more accurate response of structures subjected to impact loading. The maximum mid span deflection obtained from the proposed model under impact loading is statistically compared to the experimental dataset of tested RC beams carried out in various researches available in the literature. Furthermore, the model is then tested through experimentation work under impact testing by constructing an assembly of impact loading and Drop Hammer. A parametric study is conducted by varying the drop height of hammer and thereafter the results of mid span deflections obtained from experimental work are compared with those obtained from the proposed model to ensure the efficiency and reliability of the model.

TABLE OF CONTENTS

Page No.

LIST OF FIGURES

LIST OF TABLES

CHAPTER 1: INTRODUCTION

1.1 Introduction to Impact Loading

Throughout the course of their service life, various reinforced concrete (RC) structure components may be subjected to a variety of extreme dynamic loads, ranging from low to high rates of loading, such as earthquake, impact, and ultimately blast loading. There is a possibility that the parts of these structures could be susceptible to impact loading from various events or accidents due to the evolution of infrastructure. For instance, highway structural elements like bridge piers, side guard rails, traffic signal poles, electric distribution poles, and overhead bridge girders may experience impact from vehicle collisions. In mountainous regions, falling rocks can pose a threat to different structures. Industrial plants are at risk of critical component damage due to heavy objects falling from pipes or turbine breaks. Offshore and marine structures may face danger from ship collisions or ice impacts. Buildings of diverse types might be subjected to tornadoes or debris impact from tsunamis. Multistory building columns and bridge piers could be impacted by moving vehicles, while structures designed for protection may experience impacts from projectiles or aircraft collisions. These collisions impose significant abnormal forces on the structures, necessitating careful consideration and analysis to ensure their integrity and safety throughout their lifespan. Predicting how these structures will respond to these extreme dynamic loading is therefore crucial for better and safer design.

1.2 Factors Influencing the response of RC Beams Under Impact Loading

The response of reinforced beams under impact loading is influenced by several factors. Here are some key factors that affect their behavior:

a) **Material properties:** The mechanical properties of the materials used in the reinforced beam, such as concrete and steel reinforcement, play a crucial role. Factors like compressive strength, tensile strength, modulus of elasticity, and strain rate sensitivity determine the material's ability to withstand impact loading.

b) **Reinforcement detailing:** The arrangement, size, and spacing of reinforcement bars within the beam influence its response to impact loading. Proper reinforcement detailing can enhance the beam's resistance to dynamic loads by improving its ductility, crack control, and load distribution capacity.

c) **Beam geometry and dimensions:** The dimensions and shape of the beam, including its depth, width, and length, affect its resistance to impact loading. Beams with larger cross-sectional areas and higher aspect ratios (depth to width) generally exhibit improved load-carrying capacity and energy absorption during impact.

d) **Loading characteristics:** The magnitude, location, and duration of the impact load significantly influence the beam's response. Different types of impact loading, such as concentrated or distributed loads, can result in varying stress distributions and failure modes within the beam.

e) **Boundary conditions and supports:** The boundary conditions and support conditions of the beam affect its dynamic response. The presence of fixed or simply supported ends, restraints, or connections to other structural elements can alter the beam's behavior and the transmission of impact forces.

f) **Strain rate effects:** The strain rate at which the impact loading is applied can influence the material's response. Concrete and steel exhibit strain rate sensitivity, and their properties, including stiffness, strength, and energy absorption, may vary under different strain rates.

g) **Preloading and damage history:** The previous loading history of the reinforced beam, including any pre-existing damage or cracking, can affect its response to impact loading. Beams subjected to cyclic loading or previous damage may have reduced strength and resistance to dynamic loads.

h) **Dynamic amplification and resonance:** The dynamic behavior of the beam can lead to amplification of stresses and deflections during impact loading. Resonance phenomena, where the natural frequency of the beam aligns with the frequency of the impact load, can result in increased stresses and potential failure.

1.3 Large Displacement and Strain Rate Effect

In reinforced concrete beams, the term "strain rate sensitivity" describes how the material reacts to variations in the rate of loading or deformation. It shows how the rate at which a material is stressed or stretched affects its mechanical qualities, such as strength and stiffness. Strain rate sensitivity in the context of reinforced concrete beams is particularly important under dynamic loading circumstances, such as during earthquakes or impact events. Under these rapid loading situations, concrete's general behavior and failure mechanisms may be influenced by how sensitive it is to strain rates. Due to the presence of reinforcing steel bars, concrete is typically referred to as

a quasi-brittle material because it possesses some properties of brittle materials (such low tensile strength) as well as some ductility. The response of concrete in terms of cracking, distortion, and eventual failure can be influenced by its strain rate sensitivity. In comparison to static loading circumstances, concrete typically shows improved stiffness, strength, and energy absorption capability. Numerous mechanisms, including strain rate-dependent micro cracking, interfacial friction, and dynamic pore pressure, are thought to be responsible for this behavior.

The term "large displacement effect" in the context of impact loading describes the considerable deformations and displacements that a structure or component goes through when it is subjected to high-intensity dynamic loads. It analyzes the impact of geometric nonlinearity and describes how the structure behaves beyond small, linear elastic deformations. Due to the high magnitude and brief duration of the applied forces during impact loading, the substantial displacement effect is more noticeable. The displacements that result from the structure's deformation might grow significantly, changing the structure's geometry, stress distribution, and dynamic response. When the displacements become significant, the assumptions of small deformations and linear elasticity no longer hold. The geometric nonlinearity introduces changes in the stiffness and deformation characteristics of the structure, affecting its overall response.

1.4 Analysis of RC Beams under Impact Loading

The analysis of a structure under time-dependent short-term loading is not simple because of the complicated character of the loading and the inelastic structural response. By resolving the linear second order differential equation of motion, the system in a completely elastic viscous damping system with little displacement may be quickly and readily solved. However, the mathematics gets more difficult and non-linear in situations like an elasto-plastic system under these dynamic loading. Because the elastic component of the structural reaction occurs first when various engineered constructions, such as beams, frames, plates, or shells, are subjected to impact loads. However, a more sophisticated response of both elastic and plastic deformation is distributed along the structure when yield limit is achieved at any location. The plastic deformations are dispersed throughout the elastic, making it impossible to distinguish between them. Therefore, it is extremely difficult, and occasionally even impossible, to solve closed-form analytical problems for elasto-plastic structures. In order to obtain a rough solution, strong numerical solutions like finite element analysis (FEA) are used. [1]

Different researchers have employed different strategies to address the complexity. Among them, rigid-plastic analysis is the most straightforward and effective method and is widely accepted and applied. The limiting analysis of steel and concrete under static loads is yielding remarkable findings with this technology, and it has also demonstrated promising results when studying structures under extremely dynamic loading. Because this method disregards the elastic strain of materials, it is simple. Differential equations can be solved analytically or numerically to express the dynamic response of several types of structures, including beams, plates, shells, and others [2] for given initial and end boundary conditions. Only one fixed point or area of a structure experienced plasticity at any given time; everywhere else, rigid-body motion predominated. This rigid-plastic hypothesis is based on the presumption that energy transmitted to a structure is far greater than the energy that may be stored in strain. Because of this, using this technique to better understand how plastic deformation affects residual damage and energy absorption in ductile structures is particularly effective.

When applied to a rigid planar frame that has been subjected to impulsive or short-term pulse loading, quadratic programming has demonstrated encouraging results [2]. With the use of Newmark's integration method, the kinematic and kinetic laws are expressed in nodal or mesh descriptions, along with the plasticity relation, and are then transformed into a linear complementarity problem (LCP) [3]. Later, khan et al [4] changed the LCP's incremental form into its rate form in order to accurately depict the plasticity relation's non-holonomic nature. Second, owing to Lemke's Algorithm's reliability in handling the solution of semi-definite LCP, he substituted it for Wolfe's type solver.

1.2 Problem Statement

Current approach for evaluating the dynamic behavior of RC components such as beams by small displacement rigid plastic model have margin of improvement as large displacement and strain rate effects have not been considered in the previous modeling. Therefore, a refined model needs to be proposed by incorporating large displacement and strain rate effects in order to predict more accurate behavior of RCC beam.

1.3 Research Significance

Predicting the response of an RC beam under drop-weight impact loading is a complex phenomenon. In this regard, several approaches have been employed to predict the behavior of RCC beams under impact loading which includes Spring Mass System, Analytical approach on the basis of conservation of energy, Analytical approach on the basis of various contact laws. Application of these processes is not always simple and is occasionally impossible. Rigid plastic theory, on the other hand, is an efficient method that can be very helpful in understanding this complex behavior of RC structures. The yield stress significantly rises with an increase in the strain rate because the dynamic behavior of RC structures is very sensitive to strain rate. Any simplified model for reliably forecasting the peak response of these structures under drop-weight impact loading should take this attribute of visco-plasticity into account. Moreover, as the large displacement effect is also considered simultaneously, the complexity of the formulation can significantly increase making it quite difficult to capture the response correctly due to nonlinear effect of the forces that arises due to the large displacement effect. Therefore, it is imperative to develop a simple yet reliable model that can accurately predict the response of RC beams by considering both the large displacement effect along with the strain rate effect in order to obtain closer response in comparison with the actual one.

1.4 Research Objectives

A numerical and experimental study has been carried out on RC beams in this research in order to address the gaps and refine the previously proposed rigid plastic model which was worked out under small displacement. The main objectives of this study shall be as follows:

1. To propose a simplified model based on rigid-plasticity incorporating the large displacement along with the strain rate effect for accurately predicting the mid span deflection of Reinforced Concrete beam under impact loading
2. To validate the proposed model with the available experimental data
3. To validate the proposed model with the existing small displacement model
4. To validate the proposed model by conducting Drop Hammer Impact Experiments

CHAPTER 2: LITERATURE REVIEW

2.1 Overview

Vehicle collisions, the effect of rock falls, and terrorist operations are a few examples of the diverse engineering issues that are covered by the rapidly expanding subject of research known as impact loading response. Although RC structures are prominent almost everywhere, little is known about how these structures react to impacts. There is a lot of diversity in how response parameters are predicted according to different codes of practice such as AASHTO and British Standards, with most of them not requiring a dynamic study of the damaged RC components. But the dynamic response of RC structures, like beams, suggests that there may be situations in which the dynamic behavior differs noticeably from the static loading [5]–[7]. In fact, assessing how safe these structures are in relation to potential structural component damage requires the capacity to estimate how these structures will respond under impact loadings [8]. The majority of methods used to study the nonlinear dynamic plastic response under impact loading are complex and expensive to compute. However, due to the removal of the elastic response, rigid-plastic approximations provide a streamlined and computationally effective method for dynamic analysis [9].

When the plastic deformation is substantial, the role of elasticity in structural response can be ignored due to extreme dynamic loads. It is appropriate to consider that stress resultants on a section are coupled to deformation by a rigid-perfectly plastic constitutive law. As a result of this simple theory in impact dynamics, computationally efficient approaches have been developed that allow considerable physical insight into the underlying mechanics of motion [10]. Although a research [11] proposed using the rigid-plastic theory to solve dynamic issues, appear to have conducted the first thorough investigation in this area. This research produced a large body of literature [12]–[16] on the examinations of structures subjected to extremely dynamic loads. However, it is pertinent to mention here that, a kinematically acceptable velocity profile for the evolution of displaced configuration must be postulated for each closed-form theoretical solution.

Reinforced concrete exhibits distinct dynamic behaviors and failure modes in response to quasi static stresses, like the majority of structural materials. The large displacement effect along with the high rate of loading, which alters the material responses, is what causes this behavioral shift. The sections that follow provide a detailed explanation of this variant.

2.2 The Large Displacement Effect

The effect of changes in geometry play a crucial role when beams with axial constraint are subjected to extreme dynamic loading. Experiments were conducted by Florence and Firth [17] and Humphreys [18], on clamped beams under the action of impulse loading that was distributed evenly from where it was found that the displacements that are encountered in the beam on the termination of transition phase of motion are comparable to the depth of the beam. It has been demonstrated that membrane forces are dominant when displacements are on the order of the beam depth [19]–[22] the nature of the deformation is abruptly altered when bending action is replaced by membrane response. This suggests a significant stiffening effect in which displacements might only be a small portion of those achieved by bending alone.

In order to properly address other categories of dynamic issues, finite displacement effects must also be taken into account. Ting [23] examined a cantilever beam that had a mass attached to its tip and could withstand impact loads. He came to the conclusion that some of the discrepancy between Parkes' solution and the experiments can be attributed to neglecting the influence of finite displacements by comparing his results with Parkes' theory, in which geometry changes are not considered, and with the experimental results provided by Bodner and Symonds [24].

A rigid-plastic beam that is indefinitely long and supported on a foundation was struck transversely by a moving mass has been studied by Yu and Stronge [25]. It is demonstrated that there is no modal phase of deformation and that the transient phase moves closer to the dominant dynamic mode. Additionally, the axial forces that result from the existence of large displacements are particularly significant and their presence helps to reduce the final displacement that the infinitesimal theory would predict.

2.3 Effect of Strain Rate Sensitivity on Materials

Given that plain concrete's and the reinforcement's essential mechanical properties are greatly influenced by the strain rate impact. Therefore, the impact of strain rate on these fundamental materials over a greater range should be taken into consideration in order to accurately estimate the responses of these structures.

It is essential to take into account how different types of structures are affected by loading rates. As shown in Figure 1.1, the strain rates integrated by various loading encounters in practice have been demonstrated by Bischoff and Perry [26]. As is evident from the broad spectrum, creeping

often happens at a very modest strain rate (between 10^{-8} and 10^{-7} s^{-1}). The strain rate for static situations typically ranges from 10^{-6} to 10^{-4}/s. Additionally, during an earthquake, it may range from 10^{-3} to 1 /s, and for impact loads, it may rise to 50 /s.

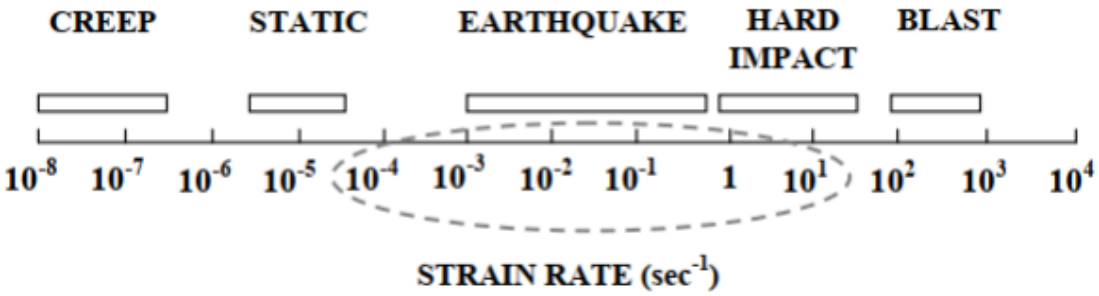

Figure 1.1: Strain Rate Pertaining to Various Loading Conditions [26]

In the blast loading regime, the strain rate that is higher than an impact scenario will decrease. Although the inertial effect on a structure is negligible during an earthquake, it is more prominent at excessive strain loading. The phenomena of impact loading is significantly complicated since it involves inertial effects, energy transfer mechanics, and the distribution of stress waves along the structure in addition to the fact that it is an extremely high dynamic loading. As a result, a number of influencing elements, including the compressive strength fc', the mass and beginning velocity of the drop hammer, and the stiffness of the contact region, have an impact on the behavior of the structure. The local failure which is the main response stage and the overall failure which corresponds to the secondary response stage which depend on high rates of loading and the propagation of stress waves, are two stages of the structural response to drop-weight impact loading.

2.3.1 Concrete

Three different elements had an impact on how the structure responded to the impact load. They are (a) the progression of cracks through time; (b) the viscous characteristics of the material between cracks; and (c) the influence of inertia on structures, which modifies stresses and strains. There are several ways to take the strain rate effect into account. The idea of Mihashi and Wittmann [27] states that when a material is loaded, cracks form on an atomic scale, and the size of these fissures grows with time. Because certain numbers of these cracks are expected to be fixed over time, long duration of loading results in more cracks than short term high loading. As a result,

while short-term high loading increases strength, long-term loading decreases it by increasing the amount of cracks in the material. The strength that is increased is expressed by following equation:

$$\frac{f_d}{f_s} = (\frac{\dot{\sigma}}{\dot{\sigma}^o})^{\alpha} \quad (2.1)$$

where f_d is dynamic strength, f_s is the static strength under the monotonic loading, $\dot{\sigma}$ is the stress rate due to dynamic load, $\dot{\sigma}^o$ is the stress rate under static loading, and α is the parameter that depends on loading, material types, and way of loading.

Reinhardt and Weerheijm have researched the impact of inertia on materials [28]. They looked at a collection of cracks that are parallel to the tension loading direction. They calculated the energy balance for this movement after noting that fracture faces move with a specific velocity when loading is applied. They discovered that the applied energy is too great to be absorbed by the fracturing process, and resultantly, the majority of the energy is retained at the fracture points. The researchers came to a conclusion on the behavior of stress distribution at the tips of the structure under various load rates based on their data. They specifically noticed that the stress distribution at the tips varies as the load rate rises. As a result, the stress intensity factor decreases as a result of this change in stress distribution. This phenomenon leads to the conclusion that materials typically show a gain in strength when subjected to high loading rates. In other words, the materials exhibit improved resistance and are able to tolerate larger amounts of stress without failing under conditions of rapid loading.

In their study, Bazant and his associates [29], [30] used a two-stage methodology to assess the impact of loading rate. They used a visco-elastic model to account for viscosity in the initial stage. They were able to study the behavior of the material under various rates of loading using this model, taking into account how the viscous qualities of the material affected how much energy was lost during the process. The second phase of the study focused on the cracks' progressive expansion. They used the activation energy theory to explain this phenomenon. This hypothesis sheds light on the processes that lead to the material's fractures gradually spreading outward under dynamic stress circumstances. It is important to note that Bazant et al.'s analysis left out the inertial effect. The dynamic response brought on by rapid loading causes a structure to experience variations in stresses and strains, which are referred to as the inertial effect. The structural reaction

to impact and high-rate loading situations should be understood, but the researchers did not take this particular feature into account in their research. The equation proposed by Bazant et al was:

$$\sigma\,(\epsilon) = \sigma^{o}\,(\epsilon)\,[1 + C_1 LN\,(\,2\dot{\epsilon}/C_2\,)] \qquad (2.2)$$

Numerous numerical studies have comprehensively investigated the compression characteristics of concrete at high loading rates over the period of several decades. The following are some important results from these studies:

Direct Relationship with Strain-Rate: Concrete's stiffness and compressive strength show a direct correlation with the strain rate at which the loading is applied. The compressive strength and stiffness of the concrete typically get better as the strain rate rises.

Impact on Different Concrete Strengths: Compared to greater strength concrete, standard strength concrete is more strongly affected by high strain rate loading. In other words, compared to high-strength concrete, the behavior of regular strength concrete is more significantly impacted by an increase in strain rate.

Moisture Sensitivity: Concrete behaves differently to high strain rates depending on its moisture sensitivity. Contrary to concrete that is wet, dry concrete is shown to be less responsive to changes in strain rate. Moisture concentration affects the way concrete reacts dynamically to high loading rates.

Slope of Stress-Strain Plot: For concrete, the descending portion of the stress-strain plot steepens as the strain rate increases. In other words, under conditions of high strain rate, the rate of decrease in stress with increasing strain becomes more dramatic.

These important discoveries provide insight into concrete's behavior under heavy loads, which is essential for engineering applications where heavy loads, collisions, or dynamic forces may occur.

When it comes to the mechanical properties of concrete, particularly its tensile strength, there is relatively limited test data available in comparison to the extensive data on its compressive strength. To study the strain rate effect on concrete in tension, researchers have utilized various testing techniques, including the cylinder split test, uniaxial direct tension test, and the Split Hopkinson Pressure Bar (SHPB) test. In one significant study, Sauris and Shah [31], they looked at how sensitive concrete is to strain rates under tension. They came to an important finding as a

result of their research: tension-versus-compression testing shows concrete to be more sensitive to strain rate.

Zielinski and Reinhardt [32] employed the Split-Hopkinson-Bar procedure to investigate the behavior of concrete and mortar paste at high strain rates. In their study, they found that the specimen treated to high-rate loading circumstances experienced significant crack formation. The overall strength of the substance increased as a result of this event. Their study revealed an interesting fact that the improvement in strength was more noticeable in concrete than in mortar. This change in behavior was attributed to concrete's inclusion of harder aggregates, which worked to stop crack growth. The concrete's strength increased as a result of a greater accumulation of stored energy in the material.

One of the most complete models for analyzing the impact of strain rate on both the compressive and tensile strength of concrete is provided by the CEB (Comité Euro-International du Béton) code. In this model, a parameter called as The Dynamic Increase Factor (DIF), is used to take into consideration how strain rate affects the behavior of the material. The dynamic increase factor (DIF) is the comparison of the static strength (strength under quasi-static or low strain rate loading) and the dynamic strength (strength under high strain rate loading). Accordingly, the expression to account the increase in compressive strength given by CEB code is as follows:

$$DIF_c = \begin{cases} \left(\frac{\dot{\epsilon}}{\dot{\epsilon_s}}\right)^{1.026\alpha_s} & \dot{\epsilon} \leq 30\ s^{-1} \\ \gamma_s \left(\frac{\dot{\epsilon}}{\dot{\epsilon_s}}\right)^{\frac{1}{3}} & \dot{\epsilon}_s > 30\ \ s^{-1} \end{cases} \tag{2.3}$$

where $\dot{\epsilon}$ is the strain rate ranges from $30 \times 10^{-6} - 300\ s^{-1}$, $\dot{\epsilon_s} = 30 \times 10^{-6}\ s^{-1}$ (the static strain-rate), $\log\ \gamma_s = 6.156\alpha_s - 2$, $\alpha s = 1/(5 + 9f_{cs}/f_{co})$, $f_{co} = 10$ MPa, f_{cs} is the static concrete compressive strength.

Malvar and Ross [46] discover that there are some differences between the old and new data, leading them to change the CEB equation for tensile strength. Following is the modified equation;

$$DIF_t = \begin{cases} \left(\frac{\dot{\epsilon}}{\dot{\epsilon}_s}\right)^{\delta} & \dot{\epsilon} \leq 1\ s^{-1} \\ \beta \left(\frac{\dot{\epsilon}}{\dot{\epsilon}_s}\right)^{\frac{1}{3}} \dot{\epsilon} & > 1\ s^{-1} \end{cases} \tag{2.4}$$

where $\dot{\epsilon}$ is the strain rate from $10^{-6}\ s^{-1} - 160\ s^{-1}$ range, $\dot{\epsilon}s = 10^{-6}\ s^{-1}$ (the static strain rate), $log\beta = 6\delta - 2$, $\delta = 1/(1 + 8f_{sc}/f_{co})$, fco = 10 MPa, fcs is the static concrete compressive strength.

To examine the impact of strain-rate and moisture content on the increased strength of concrete, Tedesco and Ross [33], [34] conducted a series of SHPB tests. The equations they suggested are listed below;

$$DIF_c = 0.00965 \log_{10} \dot{\epsilon} + 1.058 \geq 1.0 \qquad for\ \dot{\epsilon} \leq 63.1\ s^{-1} \tag{2.5}$$

and

$$DIF_c = 0.758 \log_{10} \dot{\epsilon} - 0.289 \leq 2.5 \qquad for\ \dot{\epsilon} > 63.1\ s^{-1} \tag{2.6}$$

Li and Meng [35] applied SHPB and discovered that the inertial effect on the structure increases the hydrostatic effect, which is more pronounced with increasing dynamic effect and strain rates greater than 10^2 s $^{-1}$.

The equation of Yamaguchi et al. [36] is used to incorporate the strain rate effect into the compressive strength equation provided by Drucker-Prager is:

$$DIF_c = 1.021 - 0.05076 \log_{10} \dot{\epsilon} + 0.2583 (\log_{10} \dot{\epsilon})^2 \tag{2.7}$$

By applying compressive tri-axial loading to concrete, Fujikake et al. [54] discovered a dynamic rise in the concrete's compressive strength which is as follows:

$$DIF_c = \left(\frac{\dot{\epsilon}}{\dot{\epsilon_{sc}}}\right)^{0.006\left[\log\left(\frac{\dot{\epsilon}}{\dot{\epsilon_{sc}}}\right)\right]^{1.05}} \tag{2.8}$$

where $\dot{\epsilon}_{sc} = 12 \times 10^{-5}\ s^{-1}$ and $\dot{\epsilon} < 10\ s^{-1}$

In view of above, it can be concluded that there are many equations that can be used to handle the dynamic increase in concrete's compressive and tensile strengths. However, a number of variables affect these equations' precision and utility. For instance, a number of concrete parameters, including the size of the aggregates used, the water-to-cement ratio, the amount of cement in the mix, the form of the aggregates, and even the age and curing method of the concrete, can affect the Dynamic Increase Factors (DIF). The behavior of concrete under various strain rates is affected by all of these variables. Given this complexity, it is crucial to validate these equations using a

large amount of experimental data that covers a variety of scenarios. We can make sure that the suggested equations and models are accurate and useful in practical settings by carrying out comprehensive experiments. To better understand how concrete reacts to dynamic loads, we essentially need to combine theoretical models with empirical data. By doing this, we can create prediction models that are more reliable and precise, which will be crucial when constructing secure and durable concrete structures for diverse dynamic loading scenarios.

2.3.2 Steel Reinforcement

Numerous researchers have extensively investigated the behavior of strain-rate effect on steel reinforcements. In-depth studies on the strain-rate behavior of reinforcing bars were carried out by Fu et al. [37] made important observations, noting that the yielding stress of the bar is affected by strain rate, whereas strain hardening remains largely unaffected.

Moreover, relevant discoveries were also made by Soroushian and Choi [38] on the connection between strain rate and the mechanical characteristics of steel reinforcements. In accordance with their studies, the ultimate strength of the bar exhibits less sensitivity to strain rate than the yielding stress does. However, they discovered that the material's elastic modulus is unaffected by the strain rate. Soroushian and Choi came to the conclusion that the strain rate primarily impacts the steel's static yield stress.

Furthermore, Soroushian and Choi found that different steel kinds have varying sensitivity to strain rate. Comparatively to steels with higher yielding stress, lower yielding stress steels were found to be more sensitive to fluctuations in strain rate. Malvar [39] investigated the dynamic increase factor for steel reinforcements in accordance with these findings. Malvar, in particular, found an inverse correlation between the dynamic rise factor and the bar's yielding stress. This shows that the dynamic increase factor tends to decrease as the yielding stress rises.

On the basis of the available experimental data, an equation is developed for DIFs. The following equation is applicable for strain rates ranging from 10^{-4} s^{-1} to 10 s^{-1} and yield stresses in the range of 290-710 MPa. The equation is as follows:

$$DIF_s = \left(\frac{\dot{\epsilon}}{10^{-4}}\right)^{\alpha} \tag{2.9}$$

where for yield stress, $\alpha = \alpha fy$; $\alpha fy = 0.074 - 0.04fy/414$; while for the ultimate stress, $\alpha = \alpha fu$; $\alpha fu = 0.019 - 0.009fy/414$; $\dot{\epsilon}$ is the strain rate in the form of s^{-1} and fy is the static yield strength in MPa.

2.3.3 Reinforced Concrete Beam

A simple sectional analysis method was used by Kulkarni and Shah [40] in their study to take into account the impact of strain rate on the behavior of a reinforced concrete (RC) beam. However, this method, which also took into account rate-dependent material characteristics, was unable to completely capture the shape of the stress-strain curves. The elevated bond characteristics that appear under high-rate loading situations and cause localized bar yielding to occur in an excessive way were blamed for the inadequate curve depiction. Recognizing the significance of overcoming this limitation, they devised an alternative strategy. To address this issue, Kulkarni and Shah opted to incorporate the shape of the average stress-strain curve, alongside a characterization of localized yielding. By integrating these additional elements into their analysis, they sought to achieve a more comprehensive understanding of how the RC beam responds to varying strain rates.

An innovative non-linear analytical model was presented by Fujikake et al. [41] in their novel work with the goal of precisely capturing the load-midspan deflection relationship of a reinforced concrete (RC) beam exposed to drop-weight impact. Their model incorporates the impact of strain rate on both the concrete and steel reinforcement to solve the challenges of dynamic loading. Fujikake et al. made use of the moment-curvature sectional relation of the RC beam to establish the load-deflection relationship. They made sure that a complete portrayal of the beam's response to impact loading was achieved by taking into account the impacts of strain rate on both the concrete and the steel reinforcement. This strategy enables the model to take into consideration the materials' time-dependent behavior and dynamic responses, which are essential for correctly projecting the structural performance.

In addition to this, Adhikary et al. [42] performed a numerical simulation on RC beams to examine the impact of various factors on the dynamic increase factor (DIF) and then provided two empirical formulae for the DIF.

- With Shear Reinforcements:

$$DIF = \left[1.89 - 0.067\rho_g - 0.42\rho_v - 0.14\left(\frac{a}{d}\right)\right] e^{DIF = \left[1.89 - 0.067\rho_g - 0.42\rho_v - 0.14\left(\frac{a}{d}\right)\right]} \quad (2.10)$$

- Without Shear Reinforcements:

$$DIF = \left[0.004\rho_g + 0.136\left(\frac{a}{d}\right) - 0.34\right] log_e\,\delta + \left[0.009\rho_g + 0.41\left(\frac{a}{d}\right) + 0.157\right] \qquad (2.11)$$

where ρ_g is the reinforcement of longitudinal bars, ρ_v is reinforcement ratio of the transverse bars, a/d is the shear span to the effective depth ratio, and δ is the loading rate.

2.4 Various Methods of Examining Response of RC Beam under Impact Loading

In research industry several methods have been adopted inorder to capture the response of RC Beam under impact loading. These methods include experimental setup, numerical and analytical formulation. Each of them will be discussed in successive sections.

2.4.1 Experimental Method

First Method to observe the behavior of RC beam is by forming an experimental setup for impact loading loading. In this regard, an Eight 2m long RC beams were tested by Kishi et al. under the midspan drop-weight of a 200 kg steel hammer. Cross-sectional dimensions, impact velocity, and reinforcement ratios are the variables in these tests. The author made the assumptions that the dynamic increasing factor would be 2 and that the ratio of the stored to the input energy would be 0.7 in order to design the flexure failure of the RC beam under drop-weight impact. The static bending resistance of an RC beam under impact stress was calculated using a straightforward empirical equation which is as follows:

$$P_{usd} = \frac{0.35E_{kd}}{\delta_{rd}} \qquad (2.12)$$

where P_{usd} is the static bending strength, E_{kd} is the imparted kinetic energy and δ_{rd} is the mid-span residual displacement.

Moreover, Fujikake et al. [41] conducted an impact test on twelve rectangular-shaped RC simply supported beams with cross-sectional measurements of 150 x 250 mm and 1700 mm in length. All of the beams are having reinforced section, and because their static shear to bending resistance is between 1.5 and 2.6, they all are assumed to fail in flexural. A 400 kg steel mass with a 90 mm-radius hemispherical contact tip was dropped, striking every beam. Drop-height and longitudinal reinforcement served as the variables. It was discovered that the quantity of longitudinal bars influences failure behavior. The RC beams only fails in the flexure mode for beams with fewer longitudinal bars, but fails locally near the impact site for beams with more longitudinal bars. By

strengthening the compressive reinforcement, this local failure is significantly decreased. Additionally, it was discovered that a commensurate increase in drop height significantly increases maximum impacted force, impulse, duration of the impacted load, maximum mid-span deflection, and time necessary to attain maximum mid-span deflection. However, flexural stiffness has an impact on the duration of the impacted load, the maximum deflection, and the time needed for this maximum deflection.

Tachibana et al.[43] conducted a series of low impact speed tests with span, cross-section, and longitudinal reinforcement as the variables. The striker's contact surface is curved, with a 75 mm radius. At the midpoint of the beam, steel weights of masses 150, 300, and 450 kg were employed as drop weights. As the ratio of shear resistance to bending resistance was kept greater than 1, it was anticipated that all of the beams would fail in flexure mode under static pressure. Additionally, the author creates a calculation based on the imparted energy and ultimate static flexural strength to calculate the maximum mid span deflection of the beam. The formula reads as follows:

$$\delta_{max} = 0.522 \frac{E_{col}}{Pu} \tag{2.13}$$

where δ_{max} is the maximum midspan deflection (mm), E_{col} is the imparted kinetic energy (J), Pu is the static ultimate flexural resistance (kN). This equation is valid in the range of 16.7 – 66.7 kN and 150 – 5400

The performance of RC beams were also examined under drop-weight impact loading by Chen and May [44]. He tested a total of 18 RC beams for this purpose, of which 14 have 2.7 m spans and the other 4 have 1.5 m lengths. A striker was dropped possessing a mass of 98.7 kg with a striking velocity of 7.3 m/s and all the beams were put to the test. The variables included the support conditions which were kept as simply supported and pin whereas the striker's contact surface were kept as hemispherical and flat. During testing, longitudinal reinforcements' impact force, acceleration, and strain time histories were recorded, and fracture profiles were generated from the video. Three different types of failure mechanisms were identified during testing in the reinforced concrete beams that were subjected to impact loading:

a) Flexure Failure with Cracks: In this type of failure, the beams deformed flexibly and developed cracks in the area that was affected. The concrete demonstrated the ability to endure some bending stress before failing.

b) Local Crushing and Yielding: Another type of failure involved local crushing of the concrete at the place of impact, together with yielding of the steel reinforcement. This failure mode demonstrated that the localized damage was caused when the forces concentrated at the impact point were greater than the resistance of the concrete.

c) Flexure Cracks with Scabbing: The third failure mode resembled the flexure failure discussed earlier (case a), with fractures emerging as a result of bending force. On the bottom surface of the beam, however, concrete scabbing was visible in addition to cracks. This demonstrated that the impact pressures were sufficiently strong to cause concrete pieces at the underside to separate.

From the comprehensive testing conducted, valuable conclusions were drawn regarding the factors influencing impact forces and failure modes:

a) **Support Conditions**: Surprisingly, the support conditions were found to have a relatively minor effect on the impact forces compared to other factors.
b) **Beam Length**: The length of the beams played a more significant role in determining the impact forces and failure behavior. Longer beams exhibited different responses compared to shorter ones.
c) **Behavior of Interface and Flat Head**: Interestingly, the behavior of beams with different end conditions (interface and flat head) was found to be similar under impact loading, indicating that the influence of end conditions on the structural response was limited.

2.4.2 Numerical and Analytical Method

In a study conducted by Adhikary et al [45], they developed three-dimensional finite element (FE) models of reinforced concrete (RC) beams. These models were designed to accurately represent the behavior of RC beams under various loading conditions. To ensure the reliability and accuracy of their models, they compared the simulation results with experimental data from physical testing of RC beams. Having successfully verified the FE models against experimental results, Adhikary and the team proceeded with a parametric study. The purpose of this study was to investigate and understand the influence of three key factors on the behavior of RC beams:

a) **Longitudinal Reinforcement Ratio**: This factor refers to the ratio of longitudinal steel reinforcement present in the concrete beam. By varying this ratio, they could observe its impact on the structural response and performance.

b) **Transverse Reinforcement Ratio**: The transverse reinforcement ratio represents the amount of stirrups or ties used to reinforce the RC beam. Analyzing different levels of transverse reinforcement allowed them to assess its effect on the beam's behavior.
c) **Shear Span to Effective Depth Ratio**: This ratio signifies the relative dimensions of the shear span to the effective depth of the RC beam. By varying this parameter, they could gain insights into how shear influences the structural response.

By systematically exploring these parameters, Adhikary et al. aimed to gain a deeper understanding of the factors influencing the behavior of RC beams. Such investigations contribute to the development of improved design guidelines and engineering practices, ensuring the safety and efficiency of RC structures in real-world applications. The combination of FE modeling, experimental validation, and parametric studies enables engineers to optimize the design of RC beams and enhance their performance under various loading conditions.

Saatci and Vecchio [46] employed a non-linear finite element analysis (NLFEA) approach to model reinforced concrete (RC) beams subjected to drop-weight impact loading. The efficiency of their modeling technique was evident through a comparison of time history data, specifically midspan deflection and strain in the longitudinal reinforcement, as well as the cracking profiles obtained from both NLFEA and experimental testing. By using the distributed stress field model (DSFM), the researchers achieved highly effective simulations of the response of shear critical RC beams under impact loading conditions. The DSFM incorporated the influence of strain rate-dependent material properties, making it a robust tool for capturing the dynamic behavior of the beams. Through the NLFEA procedure, Saatci and Vecchio demonstrated a significant advancement in understanding the complex behavior of RC beams under impact scenarios. The ability to validate the modeling results against experimental data highlights the accuracy and reliability of their approach. By considering strain rate effects and employing the DSFM, their modeling technique provides a comprehensive and realistic representation of the structural response to impact loading.

Zhao et al [47] developed a NLFEA using LS-DYNA with primarily default model parameters which was capable of predicting the impact responses of RC beams for both failure modes, though flexural failure is predicted with higher accuracy. In addition to this, an analytical model was also developed by Zhao et al which was based on conservation of energy and contact laws.

Fujikake et al. [41] utilized a two degrees of freedom mass-spring damping system to model reinforced concrete (RC) beams under drop-weight impact loading. This system aimed to simulate the dynamic behavior of the RC beam during impact events. The model consisted of two springs with distinct properties. The first spring represented the global stiffness of the RC beam and was obtained from the load versus midspan deflection relationship, incorporating the strain rate effect. The second spring represented the stiffness of the contact between the impacting weight and the beam, calculated using the Hertz contact theory. In terms of damping, the researchers assumed a global damping value of zero, implying no energy dissipation within the beam itself. However, for the contact spring, the damping value was considered to be half of the critical damping coefficient, allowing for some energy dissipation at the contact interface. When the model was applied to predict the response of the RC beam in cases of global flexure failure, the output was in good agreement with the impacted force, reaction force, and midspan deflection time histories. However, when it came to scenarios involving both local and global flexure failure, significant variation was observed between the model predictions and experimental data. These findings indicate that the model's accuracy is satisfactory for predicting the behavior of RC beams when global flexure failure occurs. However, it may require further refinement to effectively simulate situations where both local and global flexure failures are present. This highlights the complexity of modeling the response of RC beams under dynamic loading conditions and underscores the importance of continuously improving simulation techniques to achieve more reliable and realistic predictions for various failure scenarios.

In addition to this, Khan et al. [4], [48] used rigid plastic approach to predict the response of beam subjected to impact loading. They developed a numerical model based on kinetic, kinematic, and material plasticity relations. The resulting model took the form of a Linear Complementarity Problem (LCP), which allowed them to analyze the rigid plastic behavior of simply supported beams under impact loading conditions. However, it's worth noting that this particular numerical model had some limitations. First of all, the model was proposed just on the consideration of small displacement. Furthermore, bending-shear interaction and strain rate effect were also not taken into account. This model was further refined in a research [49] wherein bending and shear interaction were introduced in this rigid plastic model. However, the effect of large displacement and strain rate effect is still not incorporated and thus, this model has further margin of improvement for accurately predicting the response of RC beams under impact loading.

CHAPTER 3: METHODOLOGY

In this chapter, the small displacement rigid plastic model having the formulation of the Linear Complementarity Problem which was proposed by Khan et al [4] will be revised and refined by deriving a formulation for the Large Displacement along with the Strain Rate Effect. First of all the kinetic and kinematic equation for the beam shall be established. Thereafter, a relation between kinetic-kinematic equations will be formed to subsequently give the formulation for Large Displacement as a Linear Complementarity problem. Furthermore, to validate the model experimental program was conducted, so the assembly for experimental setup has also been explained in successive sections.

3.1 Nodal Description of Kinetic Equation

Consider a simply supported beam having a spans of Length L as shown in the Figure 3.1 subjected to impact loading. The mass of each of the member of the beam has been lumped at the center at a distance $\frac{L}{2}$ from each member. Out of the complete beam a single element of beam having length L has been considered in order to derive the formulation. Figure 3.3 shows the element in the original configuration and the displaced configuration. The displacements and the member end forces in the local co-ordinate system is represented by F'_m and d'_m respectively and the rotation of the element is represented by p as shown in Figure 3.3.

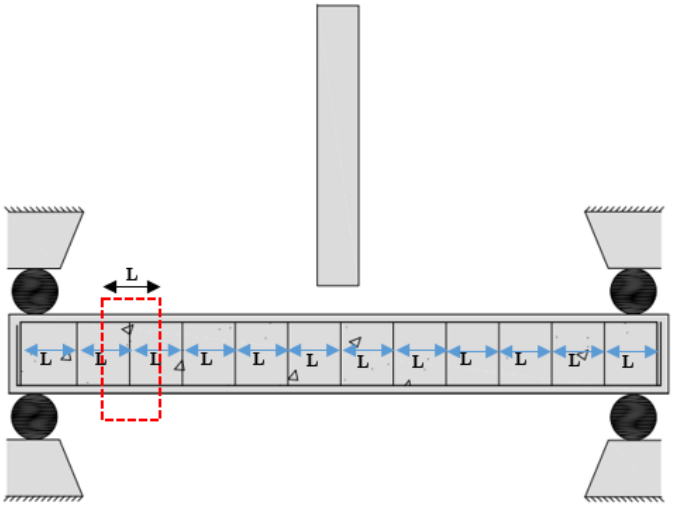

Figure 3.1: Simply Supported beam under Impact Loading

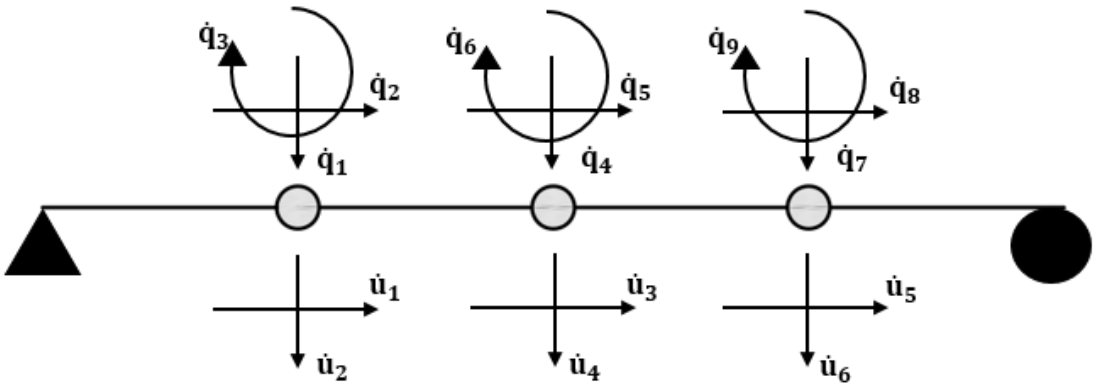

Figure 3.2: Lumped Mass Model of Beam showing Independent nodal and inertial velocities

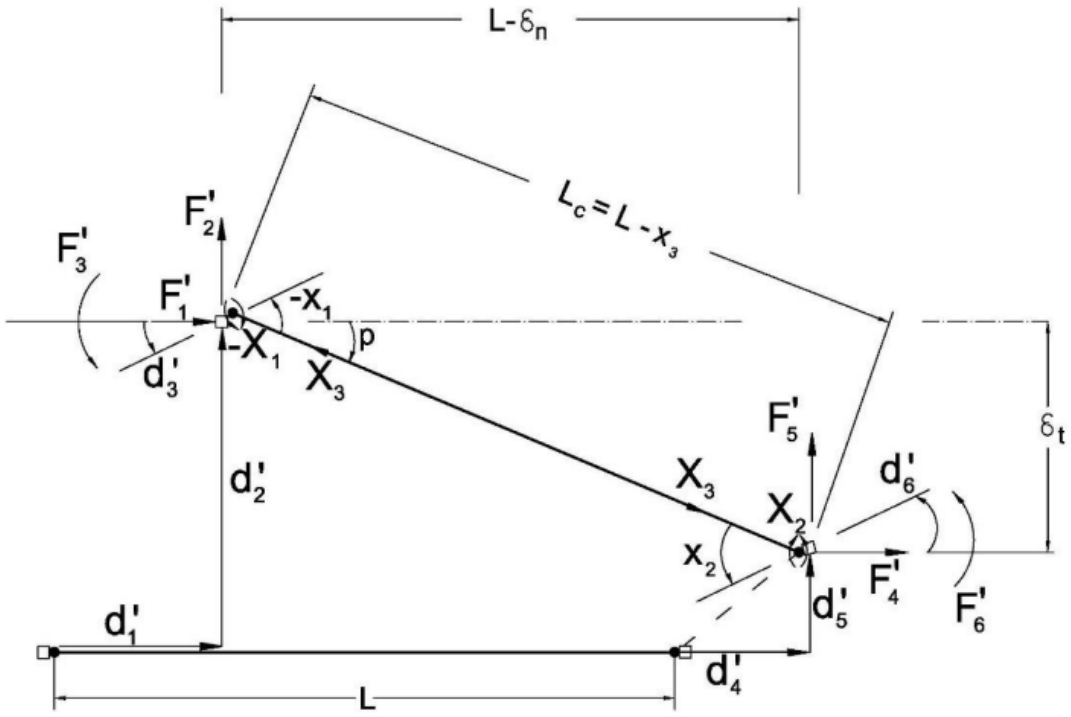

Figure 3.3: Single Beam element in Original and Displaced Configuration under Large Displacement

Now as the element or a member of a beam is removed, number of nodal forces F_{mj}'(j=1,2,3…..,m) which acts on the joint which connects each of the nodes of the beams. For one member or element of a planar beam the member forces denoted by Sm=6 and the forces that corresponds to it are shown in Figure 3.3. These forces are depicted in the local coordinate system. Furthermore, these nodal forces can be expressed in term of independent member forces denoted by Xi (i= 1,2,3,…m). Since we know that there are 3 conditions of equilibrium, therefore, the nodal forces F can be specified by 3 different independent forces X for each of the member of the beam.

In addition to these forces, when the load is distributed over the entire length of the beam stress resultants are induced at each of the members along with the independent member deformation rates.

Now, in order to maintain the equilibrium following equations are obtained:

$$\begin{bmatrix} F^{1\prime} \\ F^{2\prime} \\ F^{3\prime} \\ F^{4\prime} \\ F^{5\prime} \\ F^{6\prime} \end{bmatrix} = \begin{bmatrix} 0 & 0 & 1 \\ -L^{-1} & -L^{-1} & 0 \\ -1 & 0 & 0 \\ 0 & 0 & -1 \\ 0 & -L^{-1} & -L^{-1} \\ 0 & 1 & 0 \end{bmatrix} \begin{bmatrix} X_1 \\ X_2 \\ X_3 \end{bmatrix} - \begin{bmatrix} 1 & 0 \\ 0 & 1 \\ 0 & 0 \\ -1 & 0 \\ 0 & -1 \\ 0 & 0 \end{bmatrix} \begin{bmatrix} \pi_n \\ \pi_t \end{bmatrix} \quad (3.1)$$

Eq (3.1) can also be written as:

$$F'_m = Am^T X_m - A_{\pi m}^T \pi_m \quad (3.2)$$

And π_n and π_t are expressed as:

$$\begin{bmatrix} \pi_n \\ \pi_t \end{bmatrix} = \begin{bmatrix} \frac{s}{Lc} & -\frac{s}{Lc} & 1-c \\ -\frac{1}{L}+\frac{c}{Lc} & \frac{1}{L}-\frac{c}{Lc} & s \end{bmatrix} \begin{bmatrix} X_1 \\ X_2 \\ X_3 \end{bmatrix} \quad (3.3)$$

and s= sin(*p*) and c= cos(*p)* and *p* is the rotation of the element

Eq (3.3) can be expressed as:

$$\pi_M = Z_M X_M \quad (3.4)$$

Where π_n and π_t behaves as the additional axial and shear forces on the element and the Matrix A is a constant matrix while matrix Z is the Variable matrix which changes with respect to time based on the change in the changes in the geometry of the element. it is a function of the two

parameters p and x_3, or of δn and δt. These displacement parameters are indicated in Figure 3.3 and are expressed as:

$$p = \tan^{-1}\left(\frac{\delta_t}{L-\delta_n}\right) \tag{3.5}$$

$$Lc^2 = (L - x_3)^2 - (L - \delta_n)^2 + \delta_t^2 \tag{3.6}$$

3.2 Nodal Description of Kinematic Equation

Accordingly, as per Figure 3.3 the kinematic description for the beam element is expressed in terms of independent member deformations and displacements which are denoted by x_m and d'_m respectively:

$$\begin{bmatrix} x_1 + (p - \frac{\delta_t}{L}) \\ x_2 - (p - \frac{\delta_t}{L}) \\ x_3 + (\delta_n - x_3) \end{bmatrix} = \begin{bmatrix} 0 & -L^{-1} & -1 & 0 & L^{-1} & 0 \\ 0 & L^{-1} & 0 & 0 & -L^{-1} & 1 \\ 1 & 0 & 0 & -1 & 0 & 0 \end{bmatrix} \begin{bmatrix} d'_1 \\ d'_2 \\ d'_3 \\ d'_4 \\ d'_5 \\ d'_6 \end{bmatrix} \tag{3.7}$$

The equation can be summarized as:

$$x_m + x_{\pi m} = A_m\, d'_m \tag{3.8}$$

In this form, $x_{\pi 1}$ and $x_{\pi 2}$ are additional rotational deformations, and $x_{\pi 3}$, is an additional axial deformation, associated with the plastic zones at the ends of the member. They are expressed as:

$$\begin{bmatrix} x_{\pi 1} \\ x_{\pi 2} \\ x_{\pi 3} \end{bmatrix} = \begin{bmatrix} \frac{s}{Lc} & -\frac{1}{L} + \frac{c}{Lc} \\ -\frac{s}{Lc} & \frac{1}{L} - \frac{c}{Lc} \\ 1 - c & s \end{bmatrix} \begin{bmatrix} \delta_n \\ \delta_t \end{bmatrix} + \begin{bmatrix} R_{x1} \\ R_{x2} \\ R_{x3} \end{bmatrix} \tag{3.9}$$

Expressed as:

$$x_{\pi m} = Z_M^T\, \delta_{\pi M} + R_{\pi m} \tag{3.10}$$

Where $R_{\pi m}$ are the residuals given by:

$$R_{x1} = -R_{x2} = \rho - \frac{L\sin\rho}{L_c}, \tag{3.11}$$

$$R_{x3} = -L(1 - \cos\rho) \tag{3.12}$$

3.3 Nodal Description of Kinetic-Kinematic Equation

When a beam is divided in N number of elements, a model is created by which is represented in terms of degrees of freedom denoted by B. The degrees of freedom are selected at the junction of nodes and are expressed in terms of nodal displacement called as independent nodal velocities $\dot{q}$ as shown in Figure 3.2. In order to obtain a kinematic admissible velocity profile each of the nodal velocities are released one by one and the effect on all the other nodes are determined in terms of independent deformation rates.

Furthermore when the load $\boldsymbol{\lambda}$ is applied at the nodes of the beam it can be represented by velocities generated at each node it produces different types of forces which are the independent member forces, inertial forces and the member forces which are generated due to Large Displacement Effect which remains at equilibrium.

D'Alembert's Principle is employed in order to combine the kinetic and the kinematic equation resulting in the mathematical equation describing the kinetic-kinematic equation which is given as under:

$$\begin{bmatrix} \mathbf{0} & \mathbf{A^T} & \mathbf{A_d^T} & \mathbf{A_\pi^T} & \mathbf{A_o^T} \\ \mathbf{A} & \mathbf{0} & \mathbf{0} & \mathbf{0} & \mathbf{0} \\ \mathbf{A_d} & \mathbf{0} & \mathbf{0} & \mathbf{0} & \mathbf{0} \\ \mathbf{A_\pi} & \mathbf{0} & \mathbf{0} & \mathbf{0} & \mathbf{0} \\ \mathbf{A_o} & \mathbf{0} & \mathbf{0} & \mathbf{0} & \mathbf{0} \end{bmatrix} \begin{bmatrix} \dot{\mathbf{q}} \\ -\mathbf{X} \\ \boldsymbol{\mu} \\ \boldsymbol{\pi} \\ \boldsymbol{\lambda} \end{bmatrix} = \begin{bmatrix} \mathbf{Q = 0} \\ \mathbf{x + x_\pi} \\ \boldsymbol{\mu} \\ \boldsymbol{\delta_\pi} \\ \boldsymbol{\delta} \end{bmatrix} \tag{3.13}$$

Where, $\pi = ZX, x_\pi = Z^T\delta_\pi + R_x$ are the matrices in deformed geometry of the structure.

It is noteworthy to mention here that each of the submatrices A, A_d, A, and A_0 are comprised of the constant values which depend only on the structure's geometry based on the original configuration and the matrix Z is the matrix that depend on the geometry based in the deformed configuration and changes with the change in geometry.

Furthermore, the inertial forces can be determined by relation between The Mass matrix and their corresponding accelerations. The relation is as follows:

$$\boldsymbol{\mu} = -\mathbf{m}\ddot{\mathbf{u}} \tag{3.14}$$

Where **m** is formed by a Diagonal Matrix and $\ddot{\mathbf{u}}$ is the corresponding accelerations at the center of masses.

3.3 Plasticity Relations for Material Modelling

By establishing a link between the stress-resultant S_i^1, also known as the bending moment, and the strain-resultant rate $\dot{s}_i^1$, at the critical section i (i=1,2,3,…, n) one may derive the constitutive equation of the material model.. The yielding at the critical section i is shown in Figure 3.4 to be characterized by two variables, namely the plastic potential $\mathbf{y}_*^{\mathbf{i}}$ and the plastic deformation multiplier rate $\dot{\mathbf{x}}_*^{\mathbf{i}}$. Natural plasticity is irreversible, and complementary conditions are utilized to guarantee this process.

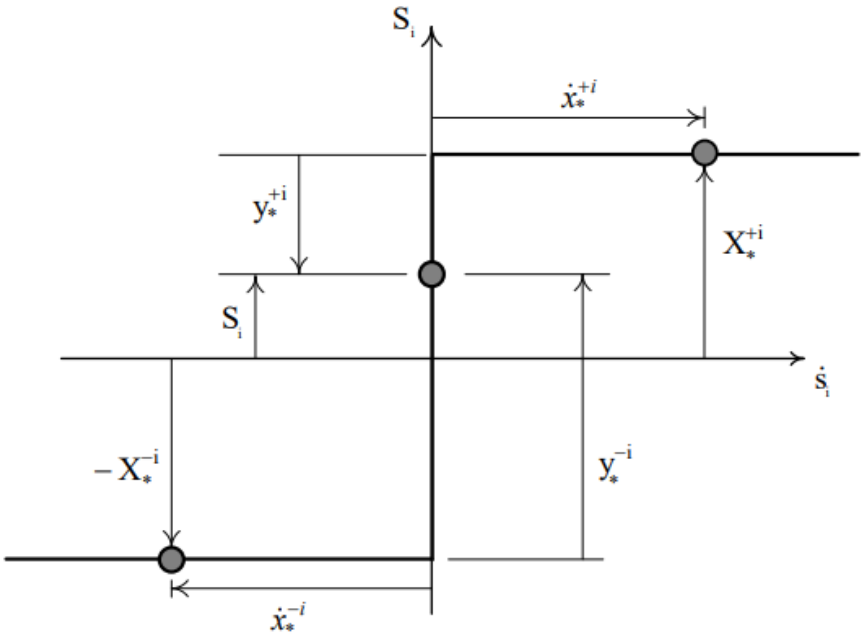

Figure 3.4: Rigid Plastic Material Modelling

The plastic potential $\mathbf{y}_*^{\mathbf{i}}$ and the plastic deformation multiplier rate $\dot{\mathbf{x}}_*^{\mathbf{i}}$ are brought together with the aid of the complementarity condition $\mathbf{y}_*^{\mathbf{T}}\,\dot{\mathbf{x}}_* = \mathbf{0}$. It means that the appropriate yield limit, $\mathbf{y}_*^{+\mathbf{i}}$**=0**, must be reached in order for the plastic deformation to take place i.e. $\dot{\mathbf{x}}_*^{+\mathbf{i}} > \mathbf{0}$. Conversely, if the yield limit is not reached, let's say $\mathbf{y}_*^{+\mathbf{i}}$**>0**, the plastic deformation cannot be active because $\dot{\mathbf{x}}_*^{+\mathbf{i}} = \mathbf{0}$.

In addition to this, the moment capacities for positive or negative bending are captured by vector $\mathbf{X}_*$. For instance, if $\mathbf{X}_*^{+\mathbf{i}} \geq \mathbf{0}$, implies that plastic deformation has taken place $(\mathbf{y}_*^{+\mathbf{i}} = \mathbf{0}, \dot{\mathbf{x}}_*^{+\mathbf{i}} \geq \mathbf{0})$ at critical section i and hence, stress resultant is positive. . A similar argument applies to $\mathbf{X}_*^{-\mathbf{i}} \geq \mathbf{0}$ which entails that $\mathbf{y}_*^{-\mathbf{i}} = \mathbf{0}$, $\dot{\mathbf{x}}_*^{-\mathbf{i}} \geq \mathbf{0}$ when $\mathbf{S}_\mathbf{1}^{\mathbf{i}}$ is negative.

In view of above discussion, the plasticity relation of a rigid perfectly plastic model can be written as:

$$\begin{bmatrix} \mathbf{0} & \mathbf{N}^{\mathbf{T}} \\ \mathbf{N} & \mathbf{0} \end{bmatrix} \begin{bmatrix} \dot{\mathbf{x}}_* \\ \mathbf{S} \end{bmatrix} + \begin{bmatrix} \mathbf{Y}_* \\ \mathbf{0} \end{bmatrix} = \begin{bmatrix} \mathbf{X}_* \\ \dot{\mathbf{s}} \end{bmatrix} \tag{3.15}$$

$$\mathbf{y}_* \geq \mathbf{0} \tag{3.16}$$

$$\mathbf{y}_*^{\mathbf{T}} \dot{\mathbf{x}}_* = \mathbf{0} \tag{3.17}$$

$$\dot{\mathbf{x}}_* = \mathbf{0} \tag{3.18}$$

where matrix **N** is expressed as **N = [I, -I]** which represents the exterior unit normal to the yield function and **I** denotes the identity matrix.

3.4 The Large Displacement Formulation

It is possible to combine the vectoral relations and the triad of complementarity conditions into a set of second-order differential equations with respect to time. However, these equations become more intricate due to the presence of the complementarity conditions. As there is no known exact solution to this type of mathematical problem, it seems logical to use a numerical approach. As a result, a time marching method is implemented to move the solution forward from one time point, t_n, to the next, t_{n+1}, where the subscript n represents consecutive discrete time intervals and t is the duration between them. Subsequently, Newmark's time-integration scheme is used to express centroidal velocities and accelerations which is as below:

$$\ddot{\mathbf{u}}_{n+1} = b_0 (\dot{\mathbf{u}}_{n+1} - \dot{\mathbf{u}}_n) - b_1 \ddot{\mathbf{u}}_n \tag{3.19}$$

$$\dot{\mathbf{u}}_{n+1} = \mathbf{u}_n + b_2 \dot{\mathbf{u}}_n + b_3 \ddot{\mathbf{u}}_n + b_4 \ddot{\mathbf{u}}_{n+1} \tag{3.20}$$

in which integration constants are

$$b_0 = 1 / \bar{\gamma} \Delta t \,, \tag{3.21}$$

$$b_1 = 1 - \bar{\gamma} / \bar{\gamma} \,, \tag{3.22}$$

$$b_2 = \Delta t, \tag{3.23}$$

$$b_3 = (0.5 - \bar{\alpha}) \Delta t, \tag{3.24}$$

$$b_4 = \bar{\alpha} \Delta t^2, \tag{3.25}$$

For rigid-plastic problems, khan et al found that one can obtain that appropriate results if $\alpha = 0.25$ and $\gamma = 0.5$.

Equations (3.14) to (3.18) are combined together, at the time $t = t_{n+1}$, and coupled with the Newmark's scheme (3.19) to (3.25) to give following the governing system:

$$\begin{bmatrix} \mathbf{b_0 M_q} & \mathbf{A_\pi^T Z - A^T} & \mathbf{0} & \mathbf{0} \\ \mathbf{A_\pi Z^T - A} & \mathbf{0} & \mathbf{TN} & \mathbf{0} \\ \mathbf{0} & \mathbf{N^T T^T} & \mathbf{0} & \mathbf{I} \end{bmatrix} \begin{bmatrix} \dot{\mathbf{q}}_{\mathbf{n+1}} \\ \mathbf{X_{n+1}} \\ \dot{\mathbf{x}}_{*\mathbf{n+1}} \\ \mathbf{y}_{*\mathbf{n+1}} \end{bmatrix} = \begin{bmatrix} -\mathbf{Y_{n+1}} \\ -\mathbf{R_x} \\ \mathbf{X}_* \end{bmatrix} \tag{3.26}$$

$$\mathbf{y}_{*\mathbf{n+1}} \geq \mathbf{0} \tag{3.27}$$

$$\mathbf{y}_{*\mathbf{n+1}}^{\mathbf{T}}\, \dot{\mathbf{x}}_{*\mathbf{n+1}} = \mathbf{0} \tag{3.28}$$

$$\dot{\mathbf{x}}_{*\mathbf{n+1}} \geq \mathbf{0} \tag{3.29}$$

with variables $\dot{\mathbf{q}}_{n+1}$, $\mathbf{X}_{n+1}$ unrestricted, the right-hand side sub-vector $\mathbf{Y}_{n+1}$ of (16) is given by:

$$\mathbf{Y_{n+1}} = -\mathbf{A_o^T}\, \boldsymbol{\lambda}_{\mathbf{n+1}} + \mathbf{A_{o(n+1)}^T} + \mathbf{b_0 M_q q_n} - (\mathbf{A_\pi^T Z - A^T})\mathbf{X_{n+1}} \tag{3.30}$$

where **matrix Z** depends upon the current position of the member and is given by:

$$\boldsymbol{Z} = \begin{bmatrix} \frac{\mathrm{S}}{\mathrm{L_c}} & \frac{-1}{\mathrm{L}} + \frac{\mathrm{c}}{\mathrm{L_c}} \\ -\frac{\mathrm{s}}{\mathrm{L_c}} & \frac{1}{\mathrm{L}} - \frac{\mathrm{c}}{\mathrm{L_c}} \\ 1 - \mathrm{c} & \mathrm{s} \end{bmatrix} \tag{3.31}$$

and $\mathbf{R_x}$ denotes Residuals given by:

$$R_{x1} = -R_{x2} = \rho - \frac{L\, sin\rho}{L_c}, \tag{3.32}$$

$$R_{x3} = -L(1 - cos\rho) \tag{3.33}$$

and mass matrix $\mathbf{M_q}$, associated with the nodal accelerations $\ddot{\mathbf{q}}$, is

$$\mathbf{M_q} = \mathbf{A_d^T m A_d} \tag{3.34}$$

The mathematical structure of the governing system eq (3.26) to (3.34) being approximated is that of a linear complementarity problem (LCP). It is important to note that the variables $[\dot{\mathbf{x}}_*, \mathbf{y}_*]$ are restricted to being complementary pairs. Additionally, the primary sub-matrix associated with

variables $[\dot{\mathbf{q}}, \mathbf{X}]$, is negative semi-definite. Hence, in order to solve the resulting LCPs lemke algorithm was used due to its simplicity and reliability.

3.5 The Strain Rate Effect

Similar to many other structural materials, RC structures are substantially stronger at extremely high rate service loads than under regular rate service loads. In these situations, the yield stress rises significantly as the straining rate increases, enabling the inclusion of strain rate effects in the dynamic plastic response [37], [42], [50] . Thus, it is imperative to incorporate the rate-dependent plastic moment into the equation given above. Notably, a substantial body of research on the strain rate-sensitive behavior at the material constitutive level is accessible. However, a little effort is made to examine the structural behavior under various loading rates. In order to account for both, the material strain-rate effect and various structural influencing parameters, the dynamic increase factor—that is, the ratio of dynamic strength to corresponding static strength—has been recommended in recent literature for use in numerical formulations.

Reinforced concrete structures exhibit substantially larger capacity to absorb energy under impact loads. According to the parametric study [51] on the dynamic increase factor (DIF), numerous material and geometric parameters can affect the strain-rate effect in these structures. On the basis of this research, two empirical equations—one with shear bar reinforcement and the other without—are suggested for the DIF of RC beams. These are as follows:

- With Shear Reinforcements:

$$DIF = \left[1.89 - 0.067\rho_g - 0.42\rho_v - 0.14\left(\frac{a}{d}\right)\right] e^{DIF=\left[1.89-0.067\rho_g-0.42\rho_v-0.14\left(\frac{a}{d}\right)\right]} \qquad (3.35)$$

- Without Shear Reinforcements:

$$DIF = \left[0.004\rho_g + 0.136\left(\frac{a}{d}\right) - 0.34\right] log_e\,\delta + \left[0.009\rho_g + 0.41\left(\frac{a}{d}\right) + 0.157\right] \qquad (3.36)$$

where ρg is the longitudinal bar reinforcement ratio, ρv is the transverse bar ratio, a/d is the ratio of shear span to effective depth, and δ is the loading rate.

It is essential to select a constitutive equation keyed to the experimental test programs in order to incorporate the aforementioned DIF equations in the plastic moment capabilities. The straightforward equation proposed by Cowper and Symonds [52] has been widely applied to the

body of research on the strain-rate effects for a variety of metal alloys, including steel and aluminum. It has been chosen to apply this equation to reinforce concrete structures in the current study based on this precedent. The equation given by copper and Symonds (23) is as follow:

$$\dot{\epsilon} = D\left(\frac{\sigma_o'}{\sigma_o} - 1\right)^p \quad , \quad \sigma_o' \geq \sigma_o \tag{3.37}$$

where σ_o' is the dynamic stresses at yielding, $\dot{\epsilon}$ is the corresponding strain rate, σ_o is the static state yield stress, and both D and p are material constants. It is of interest to note that the ratio σ_o'/σ_o can be considered as DIF straightforwardly.

Now, equation may be written as:

$$log_e\, \dot{\epsilon} = p\ log(DIF - 1) + log e\ D \tag{3.38}$$

which has the same form as a line with the parameter p as the slope, while the $log_e\ D$ as the intercept. Hence, these coefficients can be determined from the experimental data of RC structures.

By integrating through the depth (H) of rectangular cross-section beam, the above equation is reproduced by Aspden & Campbell [53] as given below

$$\frac{M_o'}{M_o} = \left\{1 + \left[\frac{H}{2z\left(1+\frac{1}{2p}\right)^p}\frac{\dot{x}}{D}\right]^{\frac{1}{P}}\right\} \tag{3.39}$$

Where z = length of plastic hinge and is calculated through

$$z = d + 0.05 \times l \tag{3.40}$$

Now, in order to incorporate strain rate sensitivity in the proposed mathematical formulation for rigid-plastic dynamics, equation for capacities at interval can be expressed as

$$\mathbf{X}_{*\mathbf{n+1}} = \mathbf{V}_n\, \mathbf{X}^{\boldsymbol{o}}{}_* \tag{3.41}$$

where $\mathbf{X}_{*\mathbf{n+1}}$ is the plastic capacity at the corresponding active node in the structural system at time $t = t_{n+1}$, $\mathbf{X}^{\boldsymbol{o}}{}_*$ is the corresponding plastic capacity for the original state of the structural material and $\mathbf{V}n$ is the viscoplastic function, evaluated at time $t = tn$.

3.6 Proposed Formulation for Large Displacement Along with Strain Rate Effect

To incorporate strain rate effect into the large displacement model Eq (3.41) shall be used, the capacity can be expressed by combining the dynamic increase factor.

Now $\boldsymbol{X}_{*\boldsymbol{n+1}}$ will become our Dynamic Moment Capacity at time n+1.

Then After employing the V_n which is our dynamic increase factor, the capacity of the beam at each interval will be increased and then the resulting governing system for Large Displacement with strain Rate effects will be as follows:

$$\begin{bmatrix} b_0 \mathrm{M_q} & \mathbf{A_\pi^T Z - A^T} & 0 & 0 \\ \mathbf{A_\pi Z^T - A} & 0 & \mathrm{TN} & 0 \\ 0 & \mathrm{N^T T^T} & 0 & \mathrm{I} \end{bmatrix} \begin{bmatrix} \dot{\mathrm{q}}_{n+1} \\ \mathrm{X}_{n+1} \\ \dot{\mathrm{x}}_{*n+1} \\ \mathrm{y}_{*n+1} \end{bmatrix} = \begin{bmatrix} -\mathrm{Y}_{n+1} \\ -\mathrm{R_x} \\ \mathbf{X}_{*\boldsymbol{n+1}} \end{bmatrix} \tag{3.42}$$

$$\boldsymbol{y}_{*n+1} \geq \mathbf{0} \tag{3.43}$$

$$\boldsymbol{y}_{*n+1}^{T} \dot{\boldsymbol{x}}_{*n+1} = 0 \tag{3.44}$$

$$\dot{\boldsymbol{x}}_{*n+1} \geq \mathbf{0} \tag{3.45}$$

3.6 Working of the Proposed Mathematical Formulation

The working of the proposed mathematical formulation has been depicted in the Figure 3.5. To start the program, first of all the matrix related to input parameters will be calculated which includes the Stiffness Matrix, Mass Matrix, Load Vector etc in Original Configuration. After that the initial deformations and capacities, Residual R and Deformed Geometry Matrix Z will be calculated at time n=0 by utilizing the initial conditions. The tabular form of the Eq (3.42) will be developed and will be solve with the help of lemke Algorithm. Using them the RHS of the Eq (3.42) all the unknown on the left hand side will be determined at time t_{n+1}. A check $|Z_{n+1}-Z_n|$ is then employed to cater any changes in geometry in the beam. Thereafter the deformations will be checked and the program will get back to induce the increased capacities by Eq (3.41) due to strain rate effect and changes in Geometry due to Large Displacement Effect by calculating Z at that interval respectively. The loop will continue until all the deformations ceases to exist which means that motion has stopped.

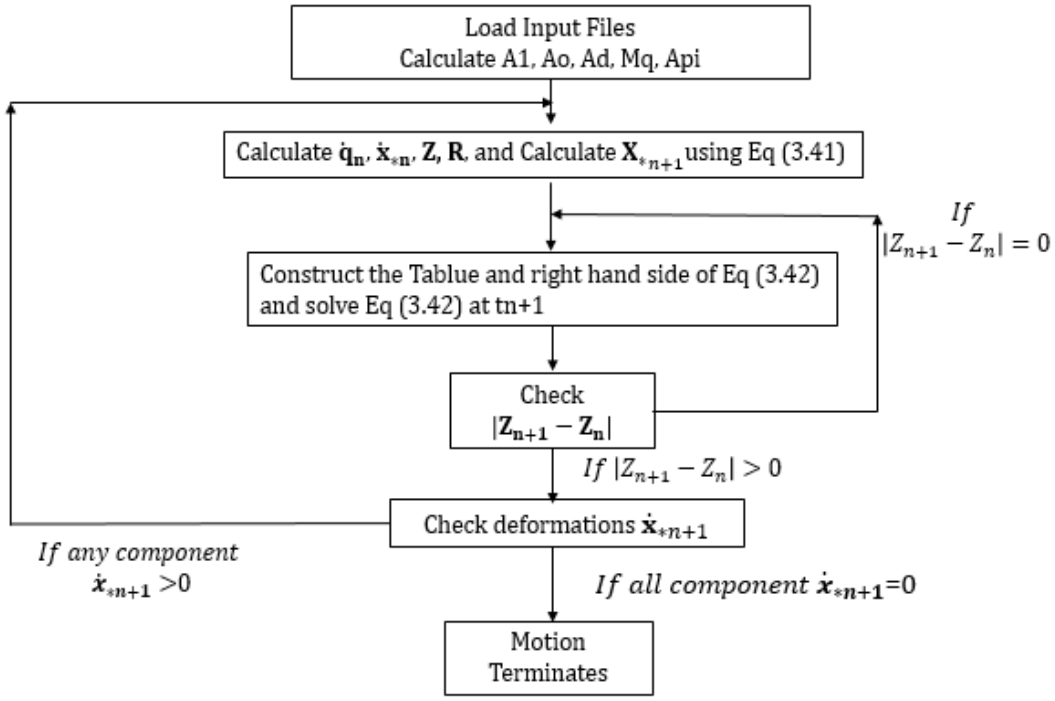

Figure 3.5: Schematic Diagram of Working of Proposed Model

3.7 Experimental Setup

3.7.1 Mix Design and Parameters of Beams

Three beams were casted to conduct a parametric study by varying the drop height of hammer. The cross section of the beam was kept 240mm by 160 mm and length was 2000 mm as shown in the Figure 3.6. The clear span between the c/c support was 1700mm. The cross section was so selected from the literature so that the beams fail in flexure.

The mix design of the ratio was kept as 1:1:2 @ 0.28 w/c ratio after several trail mixing to achieve a target strength of 40 MPa. SP-3rd Generation Superplasticizer 1.3% was used to achieve the desired strength. Table 3.1 shows the mix design kept for casting the beams.

Table 3.1: Mix Design for Beam

Description	Cement (kg/m^3)	Fine Aggregates (kg/m^3)	Coarse Aggregate (kg/m^3)	w/c Ratio	Super Plasticizer
Quantity	574	621	1284	0.28	1.3%

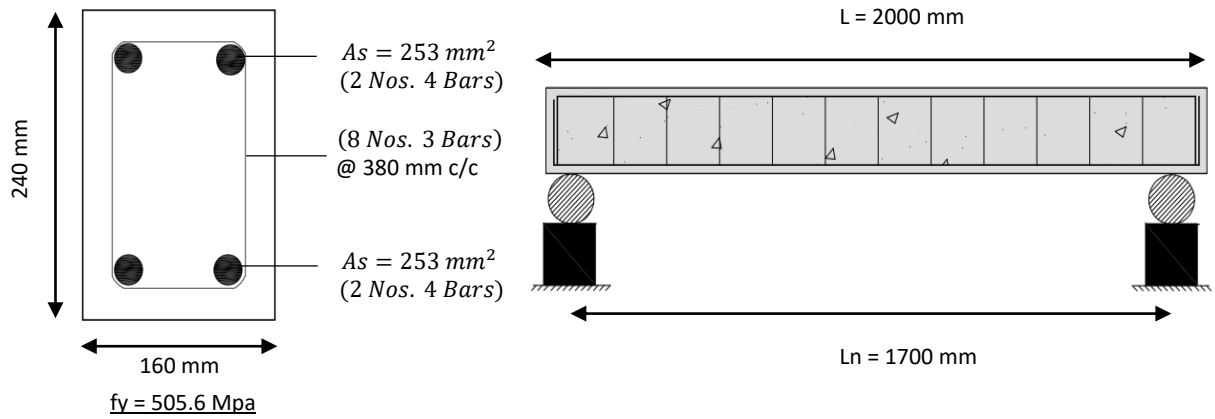

Figure 3.6: Parameters of Beam for Experimental Validation

3.7.2 Assembly for Impact Loading Test

The assembly for the impact loading test is shown in Figure 3.7. To set up the experimental setup for impact loading, first of all a hammer of 275Kg was assembled by means of steel plates of size 1m x1m of 12 plates of 20mm thickness. After the assembly of the 275-kilogram hammer using sturdy steel plates, each measuring 1x1 meter and 20mm thick, the target was to achieve accurate and controlled impact loading on the beam. To ensure precise targeting, a truss guiding assembly was meticulously installed on the supporting columns. This truss guiding assembly was installed which comprised of long steel structural elements in shape of truss that facilitated the hammer's smooth descent while maintaining its alignment with the desired center point of the beam. Moreover, to minimize friction and resistance during the hammer's free fall motion, rollers were integrated into the guiding assembly, guaranteeing a clean and unobstructed impact path. In addition to this, in order to measure the velocity of hammer a laser sensor system comprising of three lasers was installed as shown in Figure 3.7. The distance between each sensor was 150 mm. These sensors measured the time of flight of the hammer at multiple points when the hammer cut each of the laser. The hammer velocity was then calculated by calculating the change in distance over time.

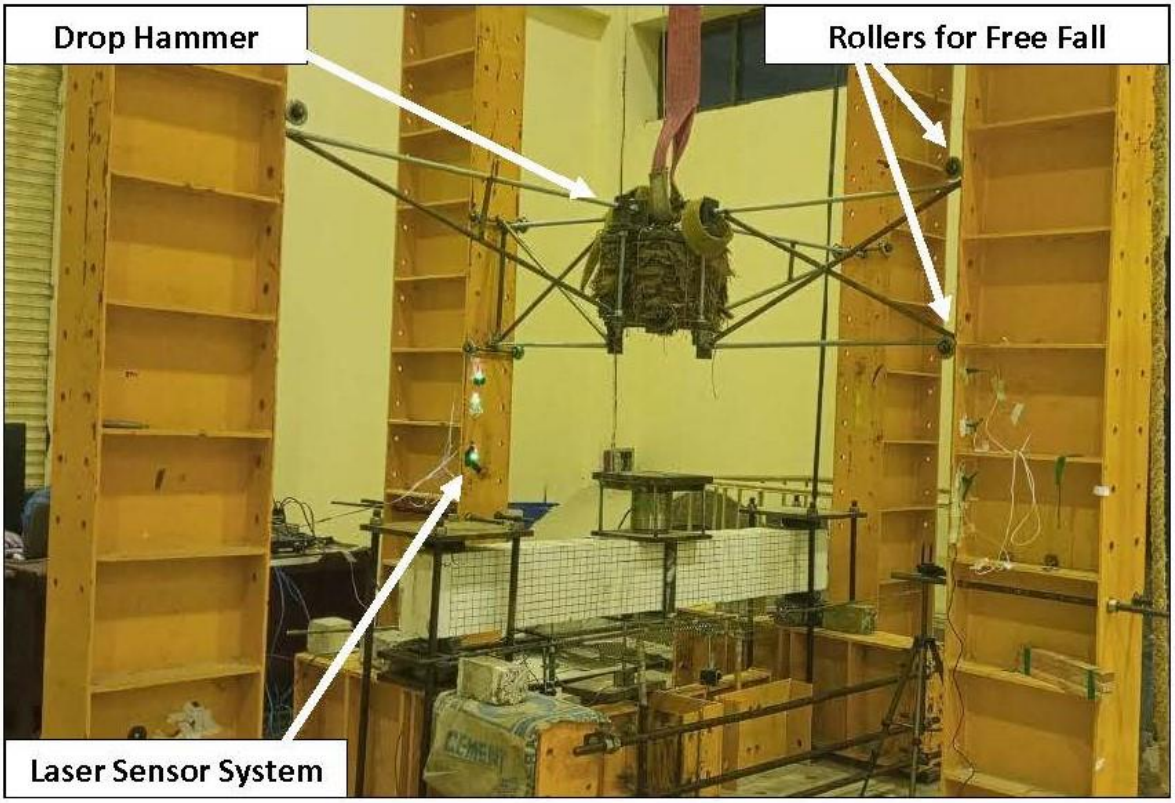

Figure 3.7: Assembly Setup for Experiments

The hammer, now suspended at the designated height, was secured in its elevated position using a rope system as shown in Figure 3.8. A rope was firmly fastened to the top of the hammer, and it was directed over a pulley, ingeniously routing its path to a predetermined anchoring point on one of the columns. This anchoring arrangement effectively held the hammer in suspension, awaiting the precise moment of release for the impact test.

Figure 3.8: Rope and Pulley System for Anchoring Hammer

In the quest to assess the beam's response to impact, a crucial aspect was to monitor the maximum deflection experienced by the beam during the loading process. For this critical measurement, a high-precision Linear Variable Differential Transformer (LVDT) was strategically installed as shown in Figure 3.9. With its ability to accurately predict displacements up to 100mm, the LVDT was precisely positioned to monitor and record the mid-span deflection of the beam as the impact event unfolded. Furthermore, to quantify the peak impact force generated by the hammer during its fall a Load Cell capable of recording loads up to an impressive 180 tons was employed. This Load Cell, carefully positioned in the setup, provided real-time measurements of the maximum force experienced by the beam during the impact. However, it is pertinent to mention here that proposed numerical model does not record the peak impact force. This force measurement provision was kept for future provision in order to further refine the current model and then verify the peak impact force using the values recorded in this experiment.

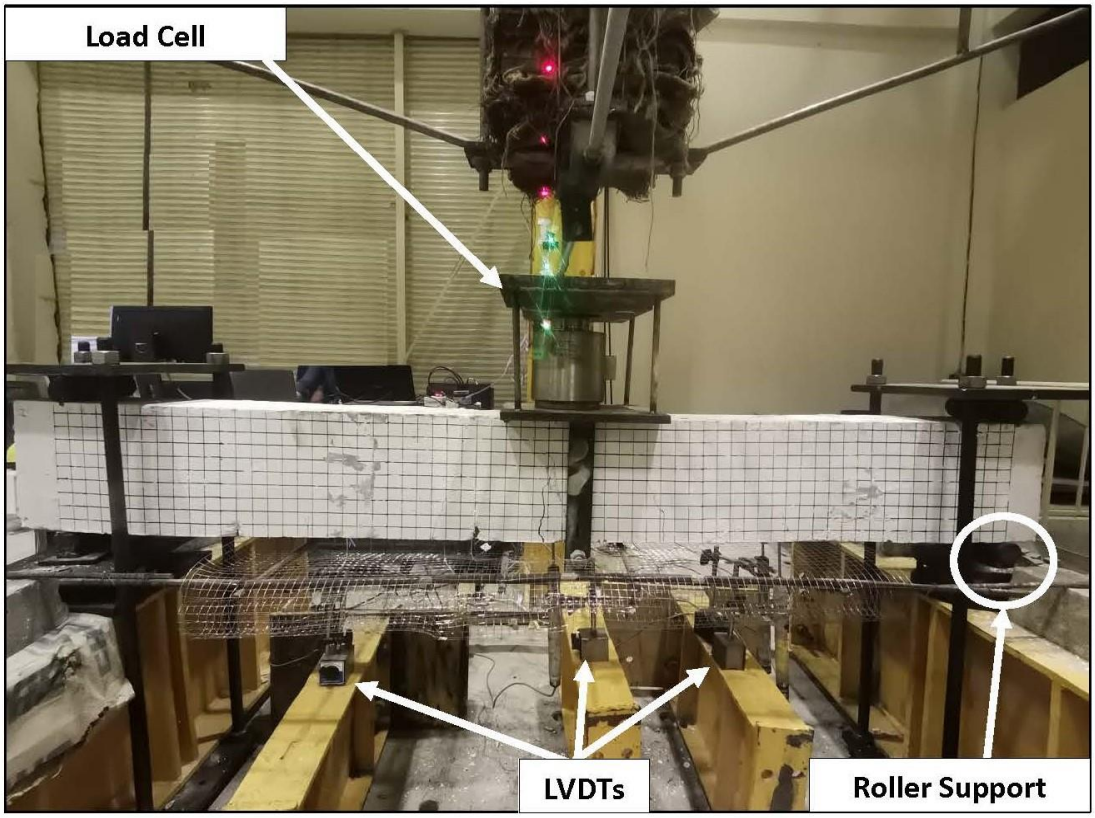

Figure 3.9: Various Instruments for Data Acquisition

To ensure the seamless acquisition of data during the experiment, a highly reliable and efficient National Instrument data logger was chosen. This state-of-the-art data logging system was equipped to record and store readings from both the Load Cell and the LVDT throughout the impact test. The data logger's precision and data storage capabilities made it an indispensable asset, as it would play a pivotal role in providing comprehensive data for post-experiment analysis and further investigation.

The combination of these meticulously selected instruments, the precise setup, and the comprehensive data collection approach ensured that the experimental impact loading test on the reinforced concrete beam was conducted with accuracy and reliability. The recorded data, encompassing both deflection measurements and applied load values, served as a foundation for in-depth analysis, offering critical insights into the beam's behavior and structural performance under impact loading conditions.

CHAPTER 4: RESULTS AND DISCUSSION

4.1 Overview

In this chapter, the validation of proposed Large displacement model incorporating Strain Rate Effect has been conducted through three different techniques i.e. Validation through available data available in literature, validation of model against small displacement model and then validation of model against the experiments conducted. Statistical analysis has been done in order to confirm the accuracy and robustness of the model.

4.2 Validation of Proposed Large Displacement Model with Strain Rate Effect

4.2.1 Experimental Database

By using a standardized set of inclusion criteria, a comprehensive experimental database of 80 simply supported Reinforced Concrete beams was carefully chosen from the literature [41], [43], [54]–[61]. The database only contains rectangular cross-sectional beams which were strike with flat or spherical contact surfaces that are subject to impact loads at the mid span. The specimens which were failing only in bending and bending-shear are included in this dataset of 80 Reinforced Concrete beams.

4.2.2 Influence Parameters of Experimental Database

This article examines the key influencing factors for RC simply supported beams. Figure 4.1 provides the influence parameters, including the impacted drop weight velocity, mass, geometric dimension of the beam, concrete compressive strength, longitudinal reinforcement, and shear reinforcement. The projectile's velocity can be seen in the figure to range from 2 to 9 meters per second, however the majority of the data are in the 3 to 7 meter per second range. Similar to the impact mass M, which ranges from 200 to 1000 kg and has a significant number of tested beams between 300 and 1000 kg. Furthermore, the width and height of RC beams fall within the range limits of 100-300 mm and 100-400 mm, respectively. The net span of simply supported RC beams spans from 1000 to 4000 mm whereas the reinforcement ratio falls in the range 0.2-0.8%. These influence parameters are shown graphically in Figure 4.1:

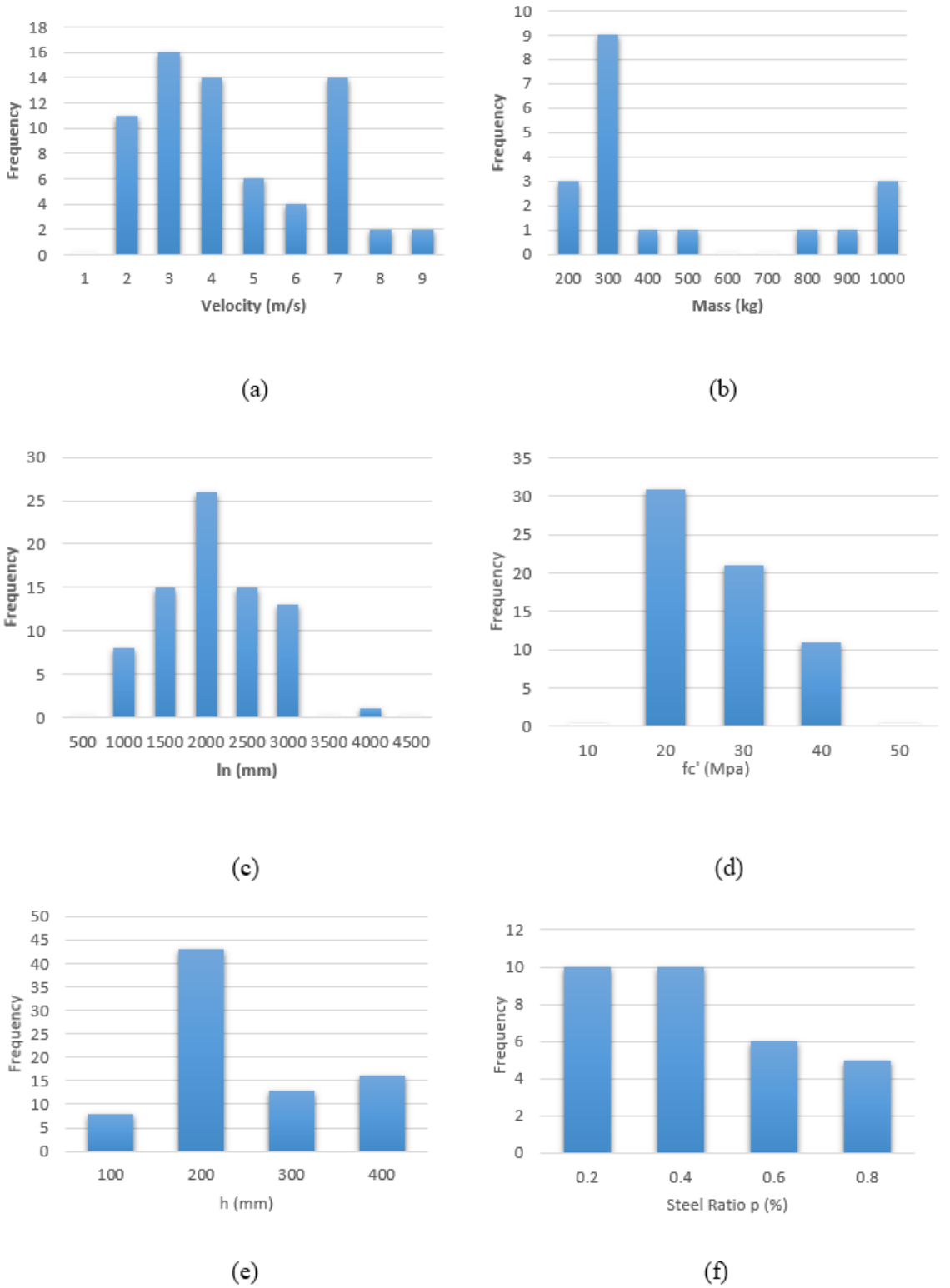

Figure 4.1: Influence Parameter of Experimental Database

4.2.3 Validation with Experimental Database

A comparative analysis is performed between the proposed LCP model incorporation large displacement and strain rate effects against the experimental data, as illustrated in Figure 4.2. To ascertain the accuracy of the LCP model using the collected dataset, a statistical assessment of midspan deflection is conducted through the use of the coefficient of determination i.e. R^2. The coefficient of determination is a variance-dependent measure, and a value close to 1 signifies excellent predictive capability. In this context, the correlation between the experimental and predicted midspan deflection is represented by an impressive R^2 value of 0.941, indicating a superior level of prediction accuracy. In addition to this, the best-fit line for the predicted peak midspan deflection follows the equation y = 0.9746x, which is remarkably close to the 45-degree benchmark. This observation suggests a strong and reliable relationship between the experimental and predicted results.

In conclusion, the statistical comparison showcases the effectiveness of the proposed LCP model, with the R^2 value of 0.941 signifying its excellent predictive capacity. The close alignment of the best-fit line with the 45-degree benchmark further reinforces the reliability of the model's predictions in relation to the experimental data. These findings validate the suitability of the LCP model for accurately predicting midspan deflection in response to impact loading scenarios.

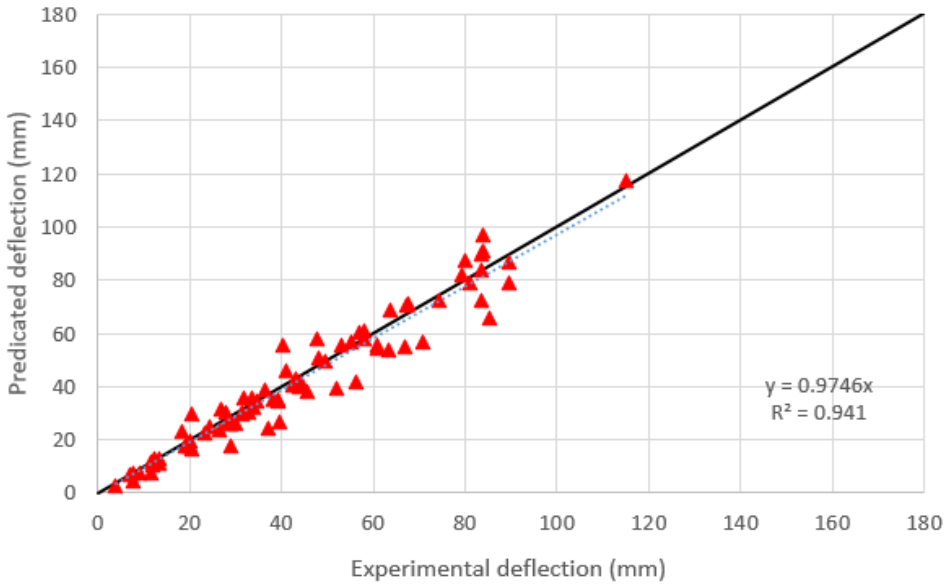

Figure 4.2: Comparison of predicted and experimental results of Maximum Midspan deflection

4.3 Validation of Proposed Model With Existing Model of Small Displacement

Table 4.1 compares the various models given by researchers using statistical parameters. It is very significant to note that the produced formulation's dependability is superior to that of all other models due to its greater value of R^2, and that its best-fit line's (m) slope is most similar to that of the benchmark line.

4.3.1 Khan et al Model of Small Displacement

The comparison of Large Displacement Model incorporating strain rate effect against model proposed by khan et al [4] is shown in Figure 4.3. The model was tested against the database of 80 RC beams for the comparison purpose.

In the evaluation of the proposed Large Displacement Model incorporating strain rate effect, the coefficient of determination i.e. R^2 was found to be an impressive 0.97. This indicates an excellent goodness of fit, demonstrating how closely the model's predictions align with the actual data. Additionally, the Average Absolute Error (AAE) was calculated to be 13.27%. Another performance metric, the average PER (Predicted to Experimental Ratio) value, was determined to be 0.98. This suggests that, on average, the model's predictions are only 2% lower or higher than the actual values. The Coefficient of Variation (CoV) associated with the average PER value is 15.37%, implying a moderate degree of variability in the PER values.

On the other hand, when examining the khan et al model [4], its coefficient of determination R^2 was found to be 0.84 which was significantly higher than the LCP model. Moreover, The Average Absolute Error (AAE) for this model was determined to be 18.06%, indicating an average deviation of 18.06% between the predicted and actual values. The mean PER value for the Khan et al model was calculated to be 1.2 which was greater than the value of 1. However, the Coefficient of Variation (CoV) associated with the mean PER value is relatively high at 24.89%, indicating a greater variability in the PER values for this model. Hence, the proposed model outperformed the small displacement model proposed by Khan et al.

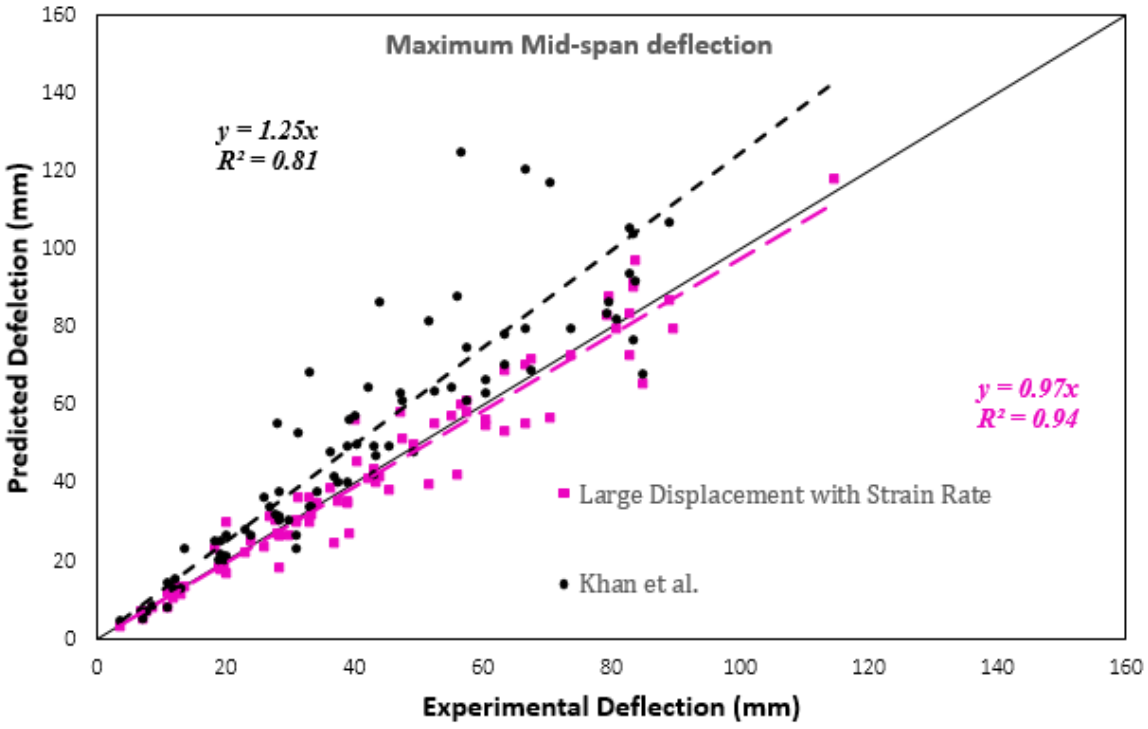

Figure 4.3: Khan et al [4] vs Proposed Model

4.3.2 Large Displacement Model Without Strain Rate Effect

A comparison between proposed Large Displacement Model incorporating strain rate effect against the Large Displacement model without strain rate was also made by removing the strain rate effect formulation from the proposed model as shown in Figure 4.4. The model was tested against the database of 80 RC beams for the comparison purpose.

In the evaluation of the proposed Large Displacement Model incorporating strain rate effect, the coefficient of determination R^2 was found to be an impressive 0.97. This indicates an excellent goodness of fit, demonstrating how closely the model's predictions align with the actual data. Additionally, the Average Absolute Error (AAE) was calculated to be 13.27%. Another performance metric, the average PER (Predicted to Experimental Ratio) value, was determined to be 0.98. This suggests that, on average, the model's predictions are only 2% lower or higher than the actual values. The Coefficient of Variation (CoV) associated with the average PER value is 15.37%, implying a moderate degree of variability in the PER values.

On the other hand, when examining the large displacement model without strain rate effect, its coefficient of determination R^2 was found to be 0.95, Though slightly lower than proposed LCP model, it still indicates a strong correlation between the model's predictions and the observed data. Moreover, The Average Absolute Error (AAE) for this model was determined to be 15.31%, indicating an average deviation of 15.31% between the predicted and actual values. The mean PER value for the large displacement model was calculated to be 0.95 which suggested that the model's predictions are 5% lower than the actual values as compared to only 2% lower of the proposed model. However, the Coefficient of Variation (CoV) associated with the mean PER value is also relatively high at 17.51% against CoV of 15.37% of proposed model, indicating a greater variability in the PER values for this model. Hence, the proposed model was showing better result against the model that was neglecting the strain rate effects.

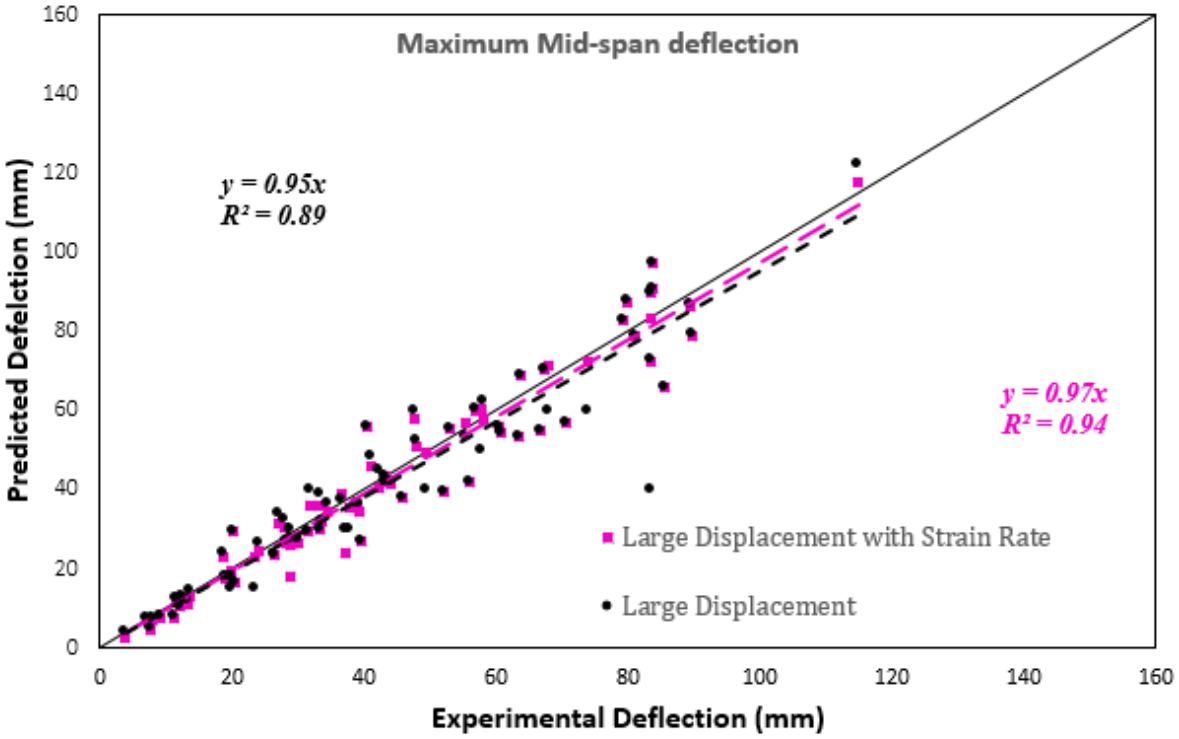

Figure 4.4: Large Displacement vs Large Displacement with Strain Rate (Proposed Model)

Table 4.1: Summary of Validation of Proposed Model against Various Models

Author	No of samples	Mean PER	Standard Deviation	COV (%)	AAE (%)	R^2
Khan et al.	80	1.2	0.3	24.89	18.06	0.84
Large displacement Model	80	0.95	0.169	17.51	15.31	0.95
Large displacement Model with Strain Rate	80	0.98	0.15	15.37	13.27	0.97

4.4 Validation of Proposed Model with Experimental Work

In order to validate the model, a parametric study was conducted by varying the height of drop hammer. The hammer was dropped from three different heights i.e. 0.7m, 1.2m, 1.7m and the displacement time histories of mid span deflection were compared with those obtained from the proposed model. In this regard three beams were casted for drop heights having the cross section of the beam as 240mm x 160 mm and length as 2000 mm as shown in the Figure 3.6. The clear span between the c/c support was 1700mm. The cross section was so selected from the literature so that the beams fail in flexure.

The cylindrical compressive strength was obtained as 40.28 MPa by casting cylinders and The flexure strength was obtained using by three point loading test giving the flexural strength of 20.46 MPa. The recorded peak impact force obtained from load cell were 286 KN, 347KN and 466KN

for drop heights 0.7m, 1.2m, 1.7m respectively whereas the Impact velocity of hammer obtained from laser sensor system were 3.46 m/s, 4.44 m/s and 5.38 m/s. The results are tabulated under Table 4.2.

Table 4.2: Results of Static and Dynamic Test on RC Beams

Description	(fc') (Mpa)	Flexure Strength (MPa)	Mass of Hammer (Kg)	Dropping Height (m)	Recoded Peak Impact Force (KN)	Impact Velocity of Hammer (m/s)
IB-1	40.28	20.46	275	0.7	286	3.46
IB-2	40.28	20.46	275	1.2	347	4.44
IB-3	40.28	20.46	275	1.7	466	5.38

4.4.1 Failure Pattern of Beams

The experiment for the impact loading test were conducted with three drop heights i.e. 0.7m, 1.2m, 1.7m. The beams cross section was so selected so that the beams fail in flexure since the proposed model was able to capture response of flexure critical beams. Figure 4.5 shows the failure pattern of beams that were subjected to drop hammer impact under various drop heights.

It can be shown from Figure 4.5 that when the drop height was 0.7m few vertical flexure cracks were appeared around the mid span indicating the flexure failure of the beam. Furthermore, when the drop height was increased to 1.2m the quantity of flexure cracks was increased and the cracks appeared to spread away from the mid span as well. Furthermore, when the drop height was kept at the maximum value of 1.7m, the cracks further increased and the depth of crack at the mid span also increased depicting the flexure failure of beams. Hence all three beams were failed under the flexure action as evident from Figure 4.5.

Failure pattern at Drop Height 0.7 m

Failure pattern at Drop Height 1.2 m

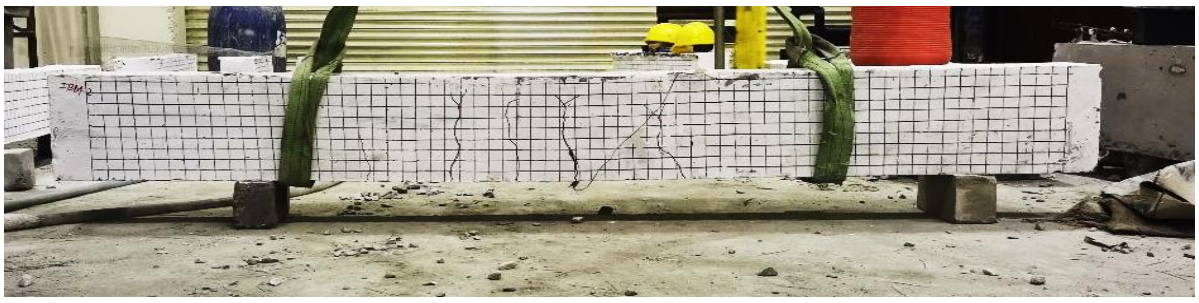

Failure pattern at Drop Height 1.7 m

Figure 4.5: Failure Pattern of Beams at Various drop heights

4.4.2 Validation of Mid Span Deflection Time Histories

Finally, the proposed model was validated by conducting a parametric study of varied drop heights by making a comparison between the time histories of the mid span deflection obtain from the experimental results and from the small displacement model of khan et al, Large Displacement Model without strain rate effect and the proposed model of Large Displacement Incorporating the Strain Rate Effect.

4.4.2.1 Progression of Mid Span Deflection of Beams under Impact Loading at Drop Height 0.7m

Figure 4.6 shows the graph of mid span deflection time histories plotted against height of drop hammer 0.7m. The black curve shows the displacement time curve obtained from the experimental results. It can be seen from Figure 4.6 that the orange curve representing the small displacement model is showing relatively large value of progression at the mid span. Furthermore, the Large Displacement model without strain rate effect shown by yellow curve depicts a slight decrease in progression of displacement due to the effect to membrane axial forces effect. Finally, the green curve shows the plot of the proposed model of large displacement with strain rate effect. It can be easily fathom from the Figure 4.6 that as both the large displacement effect and strain rate effects are considered in the model the progression of mid span displacement is decreasing due to the stiffening effect of the beams which is closer to the actualization of the experimental works.

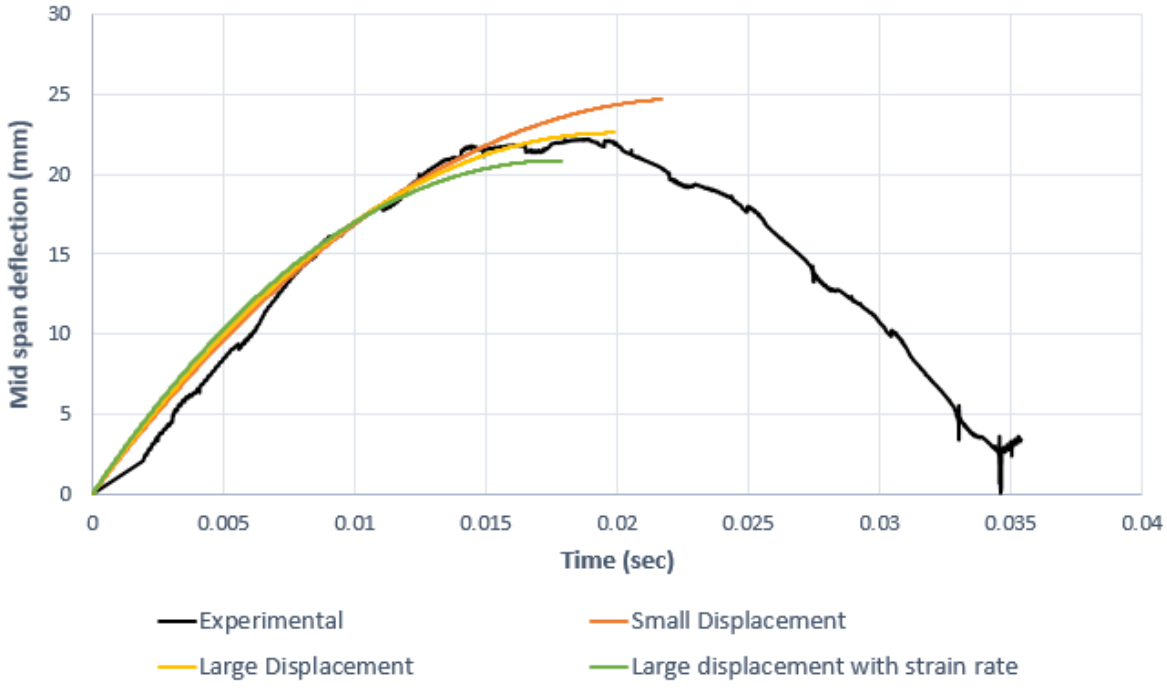

Figure 4.6: Comparison of Mid Span Deflection Histories at Drop Height 0.7m

4.4.2.2 Progression of Mid Span Deflection of Beams under Impact Loading at Drop Height 1.2m

Figure 4.7 shows the graph of mid span deflection time histories plotted against height of drop hammer at 1.2m. The black curve shows the displacement time curve obtained from the experimental results. Similar pattern of the comparison of progression of mid span deflection was seen as was obtained when the drop height of the hammer was kept 0.7m. The small displacement model curve is showing relatively large value of progression at the mid span which was followed by Large displacement model without strain rate effect and lastly the proposed model curve was showing the closest results when compared with the experiment results as evident from Figure 4.7.

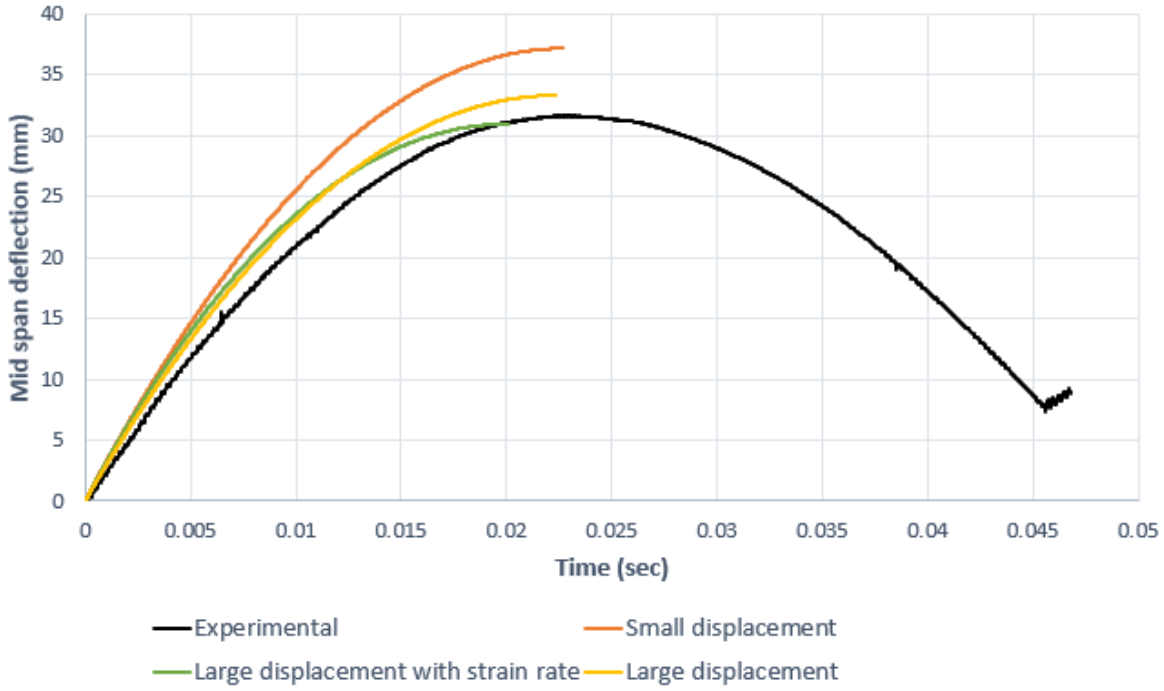

Figure 4.7: Comparison of Mid Span Deflection Histories at Drop Height 1.2m

4.4.2.3 Progression of Mid Span Deflection of Beams under Impact Loading at Drop Height 1.7m

Figure 4.8 shows the graph of mid span deflection time histories plotted against height of drop hammer at 1.7m. The black curve shows the displacement time curve obtained from the experimental results. It can be seen from Figure 4.8 that the orange curve representing the small displacement model is showing significantly large value of progression at the mid span.

Furthermore, the Large Displacement model without strain rate effect shown by yellow curve depicts a slight decrease in progression of displacement due to the effect to membrane axial forces effect. Finally, the green curve shows the plot of the proposed model of large displacement with strain rate effect. It can be easily fathom from the Figure 4.8 that as both the large displacement effect and strain rate effects are considered in the model the progression of mid span displacement is decreasing due to the stiffening effect of the beams and showing the closest results when compared to the actual results obtained from experiments. Moreover, it can also be noted that as the displacement is increasing the proposed model is showing more closer results.

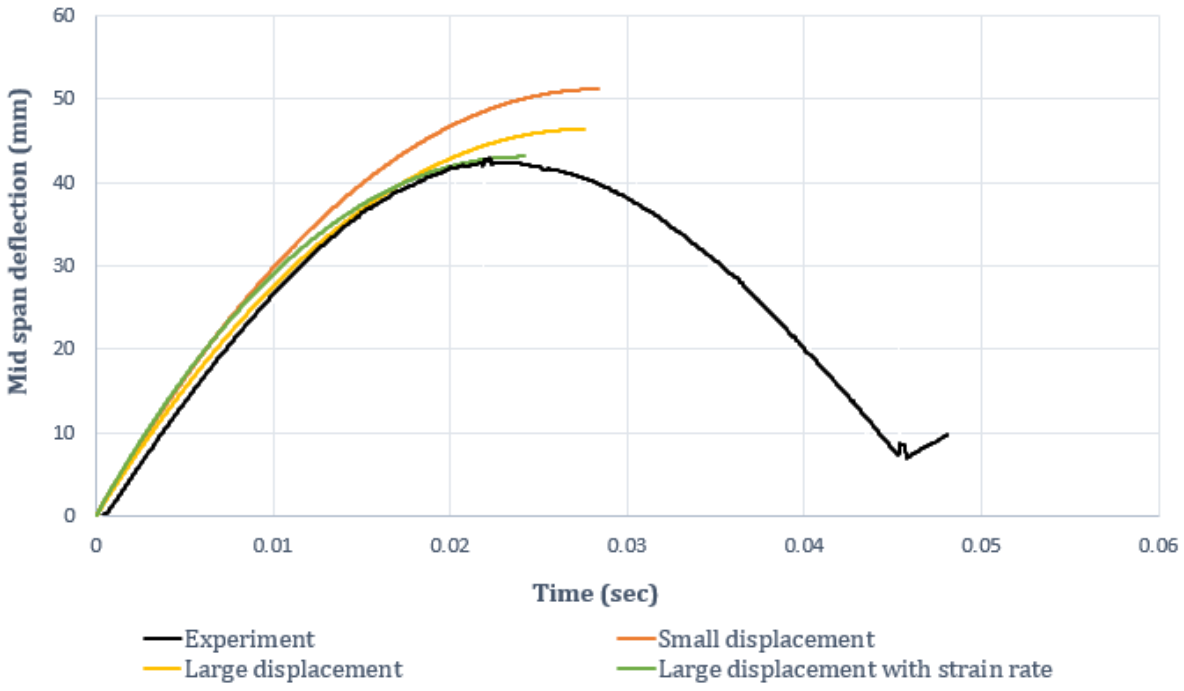

Figure 4.8: Comparison of Mid Span Deflection Histories at Drop Height 1.7m

4.4.2.4 Summary of Comparison of Maximum Mid Span Deflection

Table 4.3 shows the comparison of the mid span deflections obtained at various dropping heights of hammer from experimental test against the mid span deflections obtained through the proposed model. As per the results in Table 4.3 the maximum mid span deflection recorded for the Beams IB-1, IB-2 and IB-3 were 21.72, 32.46 and 44.63 mm respectively. The set of experiments were first run tested in the small displacement of Khan et al [4]. The results of mid span deflection obtained were 24.69, 37.23 and 52.18 mm showing an Average Absolute error of 15.09%. Subsequently, the test were run in the model comprising of large displacement without strain rate

effect. The mid span deflection of each of the beams were 22.60, 34.69 and 48.38 mm showing an an Average Absolute error of 6.43%. Finally, the experiments were run in the refined model of large displcements incorporated with the strain rate effect. The mid span deflections were respectively 20.87, 30.88 and 43.10 mm showing an Average Absolute error of 4.08%. Thus, it is can be observed that the propsed model is able to give the maximum mid span deflection with adequate accuracy given that the error is less than 5%.

Table 4.3: Summary of Maximum Mid Span Deflections

Description	**Experimental Tests**	**Small displacement**		**Large displacement without strain rate**		**Large displacement with strain rate**	
	Max Deflection (mm)	Max Deflection (mm)	AAE %	Max Deflection (mm)	AAE %	Max Deflection (mm)	AAE %
IB-1	21.72	24.69	13.70%	22.60	4.04%	20.87	3.90%
IB-2	32.46	37.23	14.66%	34.69	6.84%	30.88	4.89%
IB-3	44.63	52.18	16.91%	48.38	8.40%	43.10	3.44%
Average Absolute Error (AAE %)		**15.09%**		**6.43%**		**4.08%**	

It can be observed that the proposed model that considered only large displacement showed better results than the model of small displcement; however, the results of maximum deflection in this model were observed to be a bit higher than the experimental values. This was due to the fact that Large Dispacement only considered the second order effect due to the residual forces which occurred in the beam. Unlike the two models of small and large displacement wherein the strain rate effect has not been considered, the progression of mid span deflection of the model of large displacement with strain rate effect showed closer and more accurate progression as compared to the two models. As the mid span displacment was increasing the proposed model was predicting more closer results. The response was stiffer due to the consideration of the strain rate effect as the

capacity in the beams were changing at each interval of time thereby capturing closer and more accurate response of the beams.

CHAPTER 5: CONCLUSION AND RECOMMENDATIONS

1. An efficient method for assessing the behavior of reinforced concrete (RC) beams, particularly those that are flexure critical, under impact loading circumstances, is provided by the proposed model that incorporates large displacement along with the strain rate effect.
2. The Proposed model has been adequately refined than the previous model proposed by Khan et al and in comparison to Khan et al.'s earlier model, we can achieve more precise estimates of the maximum displacement experienced by RC beams when subjected to impact loading by including this improved model.
3. The proposed large displacement model incorporating strain rate effect key advantage is its capacity to minimize the ultimate maximum mid-span displacement when compared to predictions from the small displacement model. With the increase in mid span deflections, this benefit becomes even more prominent, demonstrating the model's greater capacity to capture accurate behavior of reinforced concrete (RC) beams under heavy loads. In practical terms, this means that the proposed model provides more realistic and conservative estimates of the mid-span displacement when subjected to severe loading scenarios. By capturing the nonlinear behavior of the RC beams more effectively, the model offers a more accurate representation of their response under extreme conditions, leading to better predictions of their structural performance.
4. The improved accuracy of the proposed model is due to the consideration of the important parameters that have a significant impact on the RC beam’s behavior when subjected to impact loading. These important parameter includes the axial forces which arises due to the non-linear effects in beam which is catered through the formulation of large displacement. Furthermore, due to the consideration of strain rate effect, the increase in capacity at each interval has been incorporated in the proposed model. Together, by considering these two factors, the response of the mid span deflections of the beam can be predicted closely to the actual response which RC usually exhibit which was evident from

the fact that the Average Absolute Error of the proposed model was less than 5% when compared to the experimental results.

5. Hence from the above discussion, it is evident that the proposed model of large displacement incorporating strain rate effect is valuable tool for engineers and researchers when designing RC beams as it can accurately predict the mid span deflection of RC beams subject to impact loading by reducing the potential for overestimating mid-span displacements thereby making the design more economical and safe.

5.1 Recommendations

Several important recommendations can be made based on the study's findings for future researches:

1. The proposed Rigid plastic model should be further modified in order to estimate the peak impact force accurately and validate the results with obtained results of peak impact force in the experimental work.

2. Extend this 1D formulation to 2D that is for plates and shell objects.

REFERENCES

[1] P. S. Symonds and W. T. Fleming, “Parkes revisited: On rigid-plastic and elastic-plastic dynamic structural analysis,” *International Journal of Impact Engineering*, vol. 2, no. 1, pp. 1–36, Jan. 1984, doi: 10.1016/0734-743X(84)90013-7.

[2] M. Capurso, “A quadratic programming approach to the impulsive loading analysis of rigid plastic structures,” *Meccanica*, vol. 7, no. 1, pp. 39–39, Jun. 1972, doi: 10.1007/BF02128839.

[3] C. L. De and M. Sahlit, “DYNAMICALLY LOADED RIGID-PLASTIC FRAMED STR UCTURES”.

[4] A. Khan, D. L. Smith, and B. A. Izzuddin, “Investigation of rigid-plastic beams subjected to impact using linear complementarity,” *Engineering Structures*, vol. 50, pp. 137–148, May 2013, doi: 10.1016/j.engstruct.2012.12.005.

[5] T. M. Pham and H. Hao, “Review of Concrete Structures Strengthened with FRP Against Impact Loading,” *Structures*, vol. 7, pp. 59–70, Aug. 2016, doi: 10.1016/j.istruc.2016.05.003.

[6] N. Kishi, H. Mikami, K. G. Matsuoka, and T. Ando, “Impact behavior of shear-failure-type RC beams without shear rebar,” *International Journal of Impact Engineering*, vol. 27, no. 9, pp. 955–968, Oct. 2002, doi: 10.1016/S0734-743X(01)00149-X.

[7] D. M. Cotsovos, “A simplified approach for assessing the load-carrying capacity of reinforced concrete beams under concentrated load applied at high rates,” *International Journal of Impact Engineering*, vol. 37, no. 8, pp. 907–917, Aug. 2010, doi: 10.1016/j.ijimpeng.2010.01.005.

[8] S. Chen, Q. Li, Y. Liu, J. Xia, and Z. Xue, “DYNAMIC ELASTOPLASTIC ANALYSIS USING THE MESHLESS LOCAL NATURAL NEIGHBOR INTERPOLATION METHOD,” *Int. J. Comput. Methods*, vol. 08, no. 03, pp. 463–481, Sep. 2011, doi: 10.1142/S0219876211002629.

[9] N. Jones, “Plastic Failure of Ductile Beams Loaded Dynamically,” *Journal of Engineering for Industry*, vol. 98, no. 1, pp. 131–136, Feb. 1976, doi: 10.1115/1.3438805.

[10] C. Cennamo, A. Gesualdo, and M. Monaco, “Shear Plastic Constitutive Behavior for Near-Fault Ground Motion,” *J. Eng. Mech.*, vol. 143, no. 9, p. 04017086, Sep. 2017, doi: 10.1061/(ASCE)EM.1943-7889.0001300.

[11] “The use of flat-ended projectiles for determining dynamic yield stress I. Theoretical considerations,” *Proc. R. Soc. Lond. A*, vol. 194, no. 1038, pp. 289–299, Sep. 1948, doi: 10.1098/rspa.1948.0081.

[12] P. S. Symonds and C. W. G. Frye, “On the relation between rigid-plastic and elastic-plastic predictions of response to pulse loading,” *International Journal of Impact Engineering*, vol. 7, no. 2, pp. 139–149, Jan. 1988, doi: 10.1016/0734-743X(88)90022-X.

[13] S. B. Menkes and H. J. Opat, “Broken beams: Tearing and shear failures in explosively loaded clamped beams,” *Experimental Mechanics*, vol. 13, no. 11, pp. 480–486, Nov. 1973, doi: 10.1007/BF02322734.

[14] W. T. Lowe, S. T. S. Al-Hassani, and W. Johnson, “Impact Behaviour of Small Scale Model Motor Coaches,” *Proceedings of the Institution of Mechanical Engineers*, vol. 186, no. 1, pp. 409–419, Jun. 1972, doi: 10.1243/PIME_PROC_1972_186_042_02.

[15] N. Mehreganian, A. S. Fallah, and L. A. Louca, “Plastic dynamic response of simply supported thick square plates subject to localised blast loading,” *International Journal of Impact Engineering*, vol. 126, pp. 85–100, Apr. 2019, doi: 10.1016/j.ijimpeng.2018.12.010.

[16] Q. Ling, Y. He, Y. He, and C. Pang, “Dynamic response of multibody structure subjected to blast loading,” *European Journal of Mechanics - A/Solids*, vol. 64, pp. 46–57, Jul. 2017, doi: 10.1016/j.euromechsol.2017.01.010.

[17] A. L. Florence and R. D. Firth, “Rigid-Plastic Beams Under Uniformly Distributed Impulses,” *Journal of Applied Mechanics*, vol. 32, no. 3, pp. 481–488, Sep. 1965, doi: 10.1115/1.3627248.

[18] J. S. Humphreys, “Plastic Deformation of Impulsively Loaded Straight Clamped Beams,” *Journal of Applied Mechanics*, vol. 32, no. 1, pp. 7–10, Mar. 1965, doi: 10.1115/1.3625788.

[19] P. S. Symonds and T. J. Mentel, “Impulsive loading of plastic beams with axial constraints,” *Journal of the Mechanics and Physics of Solids*, vol. 6, no. 3, pp. 186–202, May 1958, doi: 10.1016/0022-5096(58)90025-5.

[20] P. S. Symonds and N. Jones, “Impulsive loading of fully clamped beams with finite plastic deflections and strain-rate sensitivity,” *International Journal of Mechanical Sciences*, vol. 14, no. 1, pp. 49–69, Jan. 1972, doi: 10.1016/0020-7403(72)90006-9.

[21] T. Nonaka, “Some Interaction Effects in a Problem of Plastic Beam Dynamics—Part 1: Interaction Analysis of a Rigid, Perfectly Plastic Beam,” *Journal of Applied Mechanics*, vol. 34, no. 3, pp. 623–630, Sep. 1967, doi: 10.1115/1.3607753.

[22] J. H. Liu and N. Jones, “Dynamic response of a rigid plastic clamped beam struck by a mass at any point on the span,” *International Journal of Solids and Structures*, vol. 24, no. 3, pp. 251–270, 1988, doi: 10.1016/0020-7683(88)90032-7.

[23] T. C. T. Ting, “Large Deformation of a Rigid, Ideally Plastic Cantilever Beam,” *Journal of Applied Mechanics*, vol. 32, no. 2, pp. 295–302, Jun. 1965, doi: 10.1115/1.3625799.

[24] S. R. Bodner and P. S. Symonds, “Experimental and Theoretical Investigation of the Plastic Deformation of Cantilever Beams Subjected to Impulsive Loading,” *Journal of Applied Mechanics*, vol. 29, no. 4, pp. 719–728, Dec. 1962, doi: 10.1115/1.3640660.

[25] T. X. Yu and W. J. Stronge, “Large deflections of a rigid-plastic beam-on-foundation from impact,” *International Journal of Impact Engineering*, vol. 9, no. 1, pp. 115–126, Jan. 1990, doi: 10.1016/0734-743X(90)90025-Q.

[26] P. H. Bischoff and S. H. Perry, “Compressive behaviour of concrete at high strain rates,” *Materials and Structures*, vol. 24, no. 6, pp. 425–450, Nov. 1991, doi: 10.1007/BF02472016.

[27] H. Mihashi and F. Wittmann, “Stochastic Approach to Study the Influence of Rate of Loading on Strength of Concrete,” *HERON, 25 (3), 1980*, vol. 25, Jul. 1980.

[28] H. W. Reinhardt and J. Weerheijm, “Tensile fracture of concrete at high loading rates taking account of inertia and crack velocity effects,” in *Current Trends in Concrete Fracture Research*, Z. P. Bažant, Ed., Dordrecht: Springer Netherlands, 1991, pp. 31–42. doi: 10.1007/978-94-011-3638-9_3.

[29] Z. P. Bažant *et al.*, “Large-Strain Generalization of Microplane Model for Concrete and Application,” *J. Eng. Mech.*, vol. 126, no. 9, pp. 971–980, Sep. 2000, doi: 10.1061/(ASCE)0733-9399(2000)126:9(971).

[30] Z. P. Bažant, F. C. Caner, M. D. Adley, and S. A. Akers, “Fracturing Rate Effect and Creep in Microplane Model for Dynamics,” *J. Eng. Mech.*, vol. 126, no. 9, pp. 962–970, Sep. 2000, doi: 10.1061/(ASCE)0733-9399(2000)126:9(962).

[31] W. Suaris and S. P. Shah, “Properties of Concrete Subjected to Impact,” *J. Struct. Eng.*, vol. 109, no. 7, pp. 1727–1741, Jul. 1983, doi: 10.1061/(ASCE)0733-9445(1983)109:7(1727).

[32] A. J. Zielinski and H. W. Reinhardt, “Stress-strain behaviour of concrete and mortar at high rates of tensile loading,” *Cement and Concrete Research*, vol. 12, no. 3, pp. 309–319, May 1982, doi: 10.1016/0008-8846(82)90079-5.

[33] C. Ross and J. Tedesco, “Moisture and Strain Rate Effects on Concrete Strength,” *MJ*, vol. 93, no. 3, 1996, doi: 10.14359/9814.

[34] J. W. Tedesco and C. A. Ross, “Strain-Rate-Dependent Constitutive Equations for Concrete,” *Journal of Pressure Vessel Technology*, vol. 120, no. 4, pp. 398–405, Nov. 1998, doi: 10.1115/1.2842350.

[35] Q. M. Li and H. Meng, “About the dynamic strength enhancement of concrete-like materials in a split Hopkinson pressure bar test,” *International Journal of Solids and Structures*, vol. 40, no. 2, pp. 343–360, Jan. 2003, doi: 10.1016/S0020-7683(02)00526-7.

[36] H. Yamaguchi, K. Fujimoto, and S. Nomura, “STRESS-STRAIN RELATIONSHIP FOR CONCRETE UNDER HIGH TRIAXIAL COMPRESSION : Part 2 Rapid loading,” *Journal of Structural and Construction Engineering (Transactions of AIJ)*, vol. 396, no. 0, pp. 50–59, 1989, doi: 10.3130/aijsx.396.0_50.

[37] H. C. Fu, M. A. Erki, and M. Seckin, “Review of Effects of Loading Rate on Reinforced Concrete,” *J. Struct. Eng.*, vol. 117, no. 12, pp. 3660–3679, Dec. 1991, doi: 10.1061/(ASCE)0733-9445(1991)117:12(3660).

[38] P. Soroushian and K. Choi, “Steel Mechanical Properties at Different Strain Rates,” *J. Struct. Eng.*, vol. 113, no. 4, pp. 663–672, Apr. 1987, doi: 10.1061/(ASCE)0733-9445(1987)113:4(663).

[39] L. Malvar, “Review of Static and Dynamic Properties of Steel Reinforcing Bars,” *MJ*, vol. 95, no. 5, 1998, doi: 10.14359/403.

[40] S. Kulkarni and S. Shah, “Response of Reinforced Concrete Beams at High Strain Rates,” *SJ*, vol. 95, no. 6, 1998, doi: 10.14359/584.

[41] K. Fujikake, B. Li, and S. Soeun, “Impact Response of Reinforced Concrete Beam and Its Analytical Evaluation,” *J. Struct. Eng.*, vol. 135, no. 8, pp. 938–950, Aug. 2009, doi: 10.1061/(ASCE)ST.1943-541X.0000039.

[42] S. D. Adhikary, B. Li, and K. Fujikake, “Dynamic behavior of reinforced concrete beams under varying rates of concentrated loading,” *International Journal of Impact Engineering*, vol. 47, pp. 24–38, Sep. 2012, doi: 10.1016/j.ijimpeng.2012.02.001.

[43] S. Tachibana, H. Masuya, and S. Nakamura, “Performance based design of reinforced concrete beams under impact,” *Nat. Hazards Earth Syst. Sci.*, vol. 10, no. 6, pp. 1069–1078, Jun. 2010, doi: 10.5194/nhess-10-1069-2010.

[44] Y. Chen and I. M. May, “Reinforced concrete members under drop-weight impacts,” *Proceedings of the Institution of Civil Engineers - Structures and Buildings*, vol. 162, no. 1, pp. 45–56, Feb. 2009, doi: 10.1680/stbu.2009.162.1.45.

[45] S. D. Adhikary, B. Li, and K. Fujikake, “State-of-the-art review on low-velocity impact response of reinforced concrete beams,” *Magazine of Concrete Research*, vol. 68, no. 14, pp. 701–723, Jul. 2016, doi: 10.1680/jmacr.15.00084.

[46] S. Saatci and F. Vecchio, “Nonlinear Finite Element Modeling of Reinforced Concrete Structures under Impact Loads,” *SJ*, vol. 106, no. 5, 2009, doi: 10.14359/51663112.

[47] W. Zhao, J. Qian, and P. Jia, “Peak Response Prediction for RC Beams under Impact Loading,” *Shock and Vibration*, vol. 2019, pp. 1–12, Jan. 2019, doi: 10.1155/2019/6813693.

[48] A. Khan, M. Tariq, A. Ullah, and A. Hussain, “An Improved Linear Complementarity Solver for the Dynamic Analysis of Blast Loaded Structures,” *Int J Concr Struct Mater*, vol. 16, no. 1, p. 47, Dec. 2022, doi: 10.1186/s40069-022-00532-w.

[49] A. Khan, M. Tariq, A. Ullah, N. B. Khan, and M. Jameel, “Flexure and shear response of an impulsively loaded rigid-plastic beam by enhanced linear complementarity approach,” *Sci Rep*, vol. 12, no. 1, p. 9893, Jun. 2022, doi: 10.1038/s41598-022-14082-4.

[50] G. Gholipour, C. Zhang, and A. A. Mousavi, “Loading rate effects on the responses of simply supported RC beams subjected to the combination of impact and blast loads,” *Engineering Structures*, vol. 201, p. 109837, Dec. 2019, doi: 10.1016/j.engstruct.2019.109837.

[51] S. Das Adhikary, B. Li, and K. Fujikake, “Effects of High Loading Rate on Reinforced Concrete Beams,” *ACI Structural Journal*, vol. 111, no. 3, May 2014, doi: 10.14359/51686579.

[52] G. R. C. P. S. Symonds, “STRAIN-HARDENING AND STRAIN-RATE EFFECTS IN THE IMPACT LOADING OF CANTILEVER BEAMS,” *EROWN UNIVERSITY PROVIDENCE, R, I.*, Sep. 1957.

[53] “The effect of loading rate on the elasto-plastic flexure of steel beams,” *Proc. R. Soc. Lond. A*, vol. 290, no. 1421, pp. 266–285, Feb. 1966, doi: 10.1098/rspa.1966.0048.

[54] N. Kishi and H. Mikami, “Empirical Formulas for Designing Reinforced Concrete Beams under Impact Loading,” *SJ*, vol. 109, no. 4, 2012, doi: 10.14359/51683870.

[55] A. Q. Bhatti, N. Kishi, H. Mikami, and T. Ando, “Elasto-plastic impact response analysis of shear-failure-type RC beams with shear rebars,” *Materials & Design*, vol. 30, no. 3, pp. 502–510, Mar. 2009, doi: 10.1016/j.matdes.2008.05.068.

[56] L. Jin, R. Zhang, G. Dou, J. Xu, and X. Du, “Experimental and numerical study of reinforced concrete beams with steel fibers subjected to impact loading,” *International Journal of Damage Mechanics*, vol. 27, no. 7, pp. 1058–1083, Jul. 2018, doi: 10.1177/1056789517721616.

[57] D.-B. Zhao, W.-J. Yi, and S. K. Kunnath, “Shear Mechanisms in Reinforced Concrete Beams under Impact Loading,” *J. Struct. Eng.*, vol. 143, no. 9, p. 04017089, Sep. 2017, doi: 10.1061/(ASCE)ST.1943-541X.0001818.

[58] S. D. Adhikary, B. Li, and K. Fujikake, “Low Velocity Impact Response of Reinforced Concrete Beams: Experimental and Numerical Investigation,” *International Journal of Protective Structures*, vol. 6, no. 1, pp. 81–111, Mar. 2015, doi: 10.1260/2041-4196.6.1.81.

[59] Xu B, Zeng X. Experimental study on the behaviors of reinforced concrete beams under impact loadings. Tumu Gongcheng Xuebao/China Civ Eng J 2014;47.

[60] Zhao DB, Yi WJ. Anti-impact behavior and design method for RC beams. Zhendong Yu Chongji/JournalVibShock 2015;34:139–45. https://doi.org/10.13465/j.cnki.jvs.2015.11.025.

[61] Dou G, Du X, Li L. Experimental study on the behavior of high strength reinforced concrete beams under impact load. Tianjin Daxue Xuebao (Ziran Kexue Yu Gongcheng Jishu Ban)/Journal Tianjin Univ Sci Technol 2014;47:1072–80. https://doi.org/10.11784/tdxbz201403083.